Lithos 117 (2010) 119–134

Contents lists available at ScienceDirect

Lithos

journal homepage: www.elsevier.com/locate/lithos

Origin of the giant Allard Lake ilmenite ore deposit (Canada) by fractional crystallization, multiple magma pulses and mixing

Bernard Charlier *, Olivier Namur, Simon Malpas, Cédric de Marneffe, Jean-Clair Duchesne, Jacqueline Vander Auwera, Olivier Bolle

Department of Geology, University of Liège, 4000 Sart Tilman, Belgium

ARTICLE INFO

Article history:
Received 27 October 2009
Accepted 12 February 2010
Available online 21 February 2010

Keywords:
Grenville
Lac Tio
Titanium ores
Cumulates
Sapphirine

ABSTRACT

The late-Proterozoic Allard Lake ilmenite deposit is located in the Havre-Saint-Pierre anorthosite complex, part of the allochtonous polycyclic belt of the Grenville Province. Presently the world's largest Fe–Ti oxide deposit, it had a pre-mining amount in excess of 200 Mt at grades over 60 wt.% hemo-ilmenite. The main ore body is a funnel-shaped intrusion, measuring 1.03 × 1.10 km and 100–300 m-thick. Two smaller bodies are separated by faults and anorthosite. The ore is an ilmenite-rich norite (or ilmenitite) made up of hemo-ilmenite ($Hem_{22.6–29.4}$, 66.2 wt.% on average), andesine plagioclase ($An_{45–50}$), aluminous spinel and locally orthopyroxene. Whole-rock chemical compositions are controlled by the proportions of ilmenite and plagioclase ± orthopyroxene which supports the cumulate origin of the deposit. Ore-forming processes are further constrained by normal and reverse fractionation trends of Cr concentration in cumulus ilmenite that reveal multiple magma emplacements and alternating periods of fractional crystallization and magma mixing. Mixing of magmas produced hybrids located in the stability field of ilmenite resulted in periodic crystallization of ilmenite alone. The unsystematic differentiation trends in the Allard Lake deposit, arising from a succession of magma pulses, hybridisation, and the fractionation of hemo-ilmenite alone or together with plagioclase suggest that the deposit formed within a magma conduit. This dynamic emplacement mechanism associated with continuous gravity driven accumulation of Fe–Ti oxides and possibly plagioclase buoyancy in a fractionating ferrobasalt explains the huge concentration of hemo-ilmenite. The occurrence of sapphirine associated with aluminous spinel and high-alumina orthopyroxene (7.6–9.1 wt.% Al_2O_3) lacking exsolved plagioclase supports the involvement of a metamorphic overprint during the synchronous Ottawan orogeny, which is also responsible for strong textural equilibration and external granule of exsolved aluminous spinel due to slow cooling.

1. Introduction

An ilmenite deposit (50.67°N, 63.67°W) was discovered in June 1946 in the Allard Lake area near a small lake named Lac Tio during the first aeromagnetic survey for ore exploration (Bourret, 1949). It is located 43 km northeast of Havre-Saint-Pierre in Quebec. Following two years of intensive drilling by Kennco Explorations, it has been continuously exploited since 1951 as an open-pit mine. Presently, it is the world's largest hard-rock ilmenite deposit and contributed 12–17% of the world ilmenite production these last 5 years (U.S.G.S., 2010). The hemo-ilmenite ore body has also been intensively studied for its large remanent magnetic anomaly (Carmichael, 1959; Hargraves, 1959; McEnroe et al., 2007).

The Allard Lake ilmenite deposit is situated in the Havre-Saint-Pierre anorthosite complex that is part of the AMCG suites (Anorthosite–Mangerite–Charnockite–(rapakivi) Granite) of the Grenville Province where there are many occurrences of Fe–Ti–P ores (Dymek and Owens, 2001; Hébert et al., 2005; Morisset et al., submitted for publication). This deposit has usually been considered to have formed as an enormous drop of immiscible Fe–Ti-enriched liquid separated from the magma remaining from the crystallization of the andesine anorthosite (Hammond, 1952; Lister, 1966), a mechanism that has also been proposed for other Fe–Ti deposits (Bateman, 1951; Philpotts, 1967; Kolker, 1982; Force, 1991; Zhou et al., 2005). This model, however, comes up against the inadequacy of immiscibility to produce monomineralic rocks and support for the possible early saturation of Fe–Ti oxides (e.g. Duchesne, 1999; Charlier et al., 2009), evidenced by the occurrence of plagioclase-ilmenite cumulates at the base of stratigraphic sequences in the Tellnes deposits (Charlier et al., 2006) and in the Bjerkreim-Sokndal layered intrusions (Wilson et al., 1996) and by the presence of abundant Fe–Ti oxide inclusions in primitive cumulus olivine from the Panzhihua intrusions (Pang et al., 2008, 2009). Moreover, specific experiments on immiscibility (Lindsley, 2003) have even

* Corresponding author. Tel.: +32 4 3662250; fax: +32 4 3662029.
E-mail address: b.charlier@ulg.ac.be (B. Charlier).

0024-4937/$ – see front matter © 2010 Elsevier B.V. All rights reserved.
doi:10.1016/j.lithos.2010.02.009

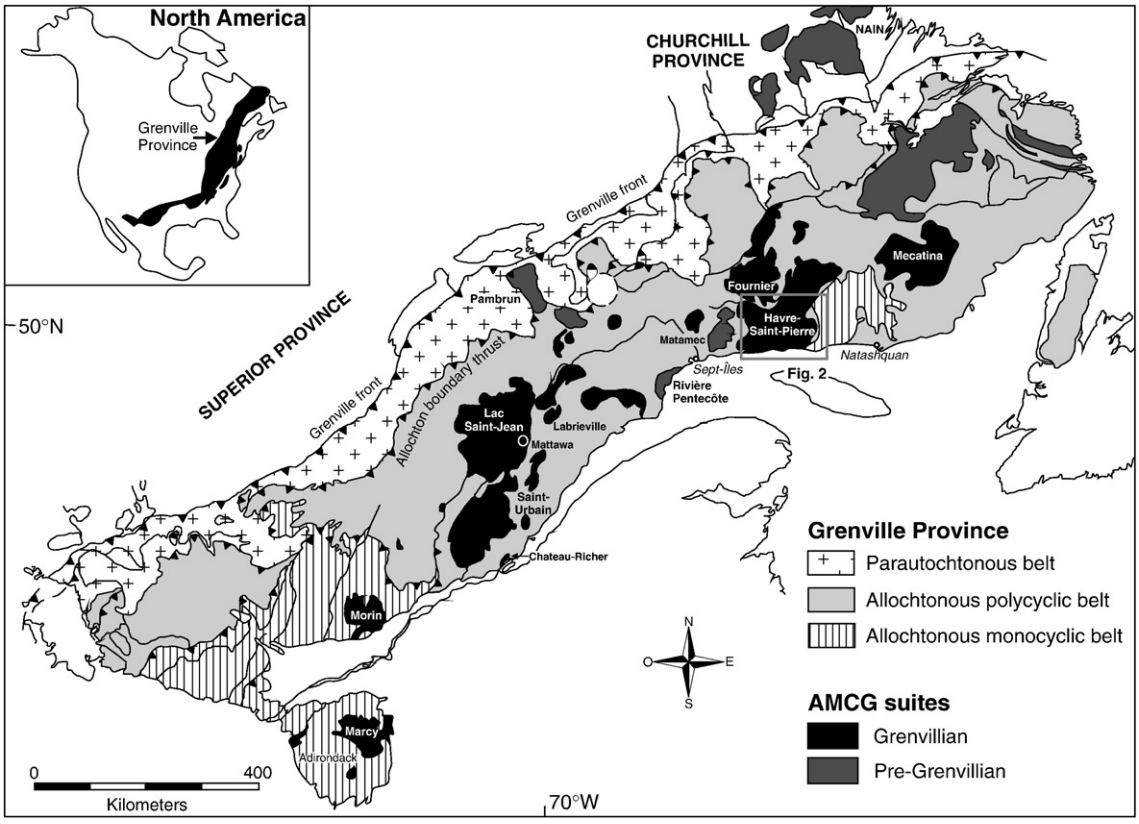

Fig. 1. Simplified geological map of the Grenville Province showing the geological subdivisions into parautochtonous and allochtonous belts (after Rivers et al., 1989; Davidson, 1995; Wodicka et al., 2003; Corriveau et al., 2007) and the major Proterozoic pre-Grenvillian and Grenvillian anorthosite–mangerite–charnockite–granite suites.

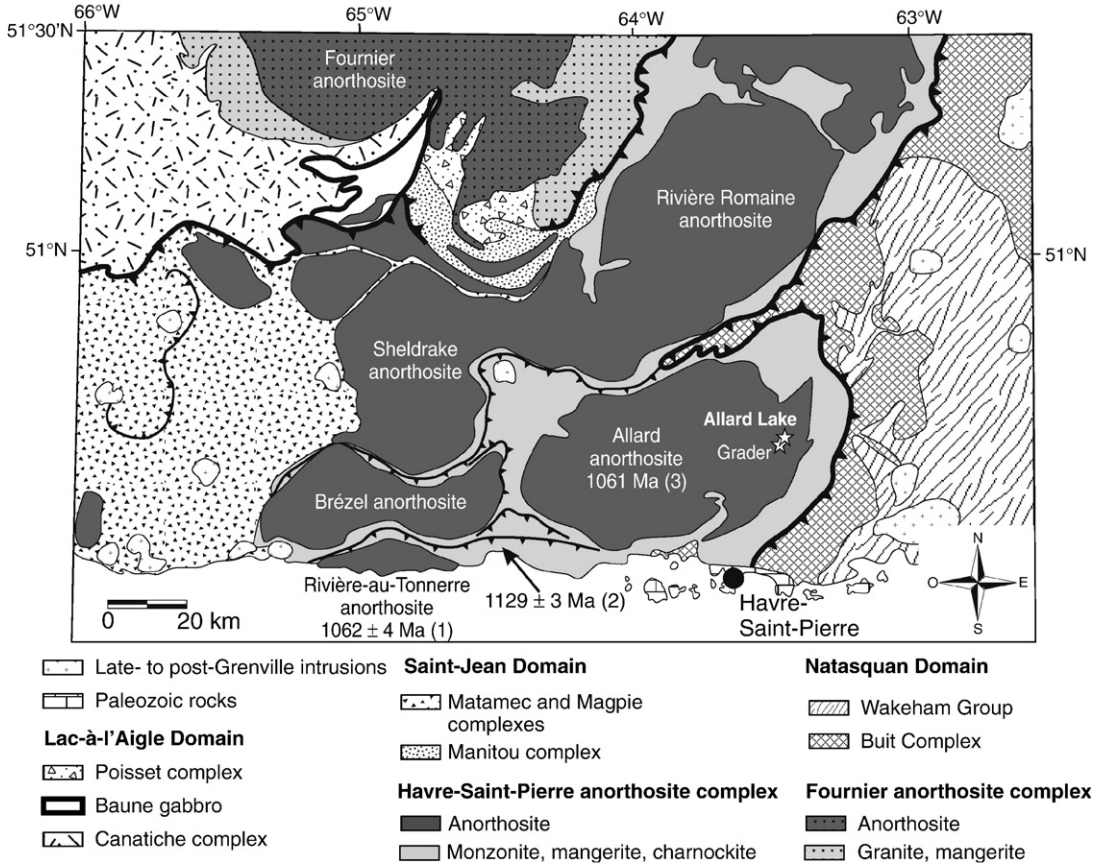

Fig. 2. Geological map of the Havre-Saint-Pierre anorthosite complex (after Gobeil et al., 2003; Wodicka et al., 2003; Morisset et al., 2009), with location of the Allard Lake deposit and the Grader layered intrusion and geochronological data. (1) van Breemen and Higgins (1993); (2) Emslie and Hunt (1990); (3) Morisset et al. (2009).

concluded that Fe–Ti oxide melts do not exist. However, the detailed mechanism of formation of huge amounts of ilmenite ore remains uncertain. Plagioclase buoyancy has been invoked in the Tellnes ilmenite deposit (SW Norway; Charlier et al., 2007) and the Grader layered intrusion (Canada; Charlier et al., 2008) to explain the discrepancy between the inferred cotectic proportion of ilmenite (around 15–20 wt.%) and the much higher proportion of ilmenite in the cumulates. However, in these occurrences, the concentration of ilmenite only ever reaches higher proportions than 50 wt.% locally in thin layers, while the Allard Lake deposit contains more than 100 Mt of ore with >75 wt.% hemo-ilmenite.

Chemical analyses on new samples from the Allard Lake deposit and an extensive mining database are used in this contribution to illuminate the crystallization processes that have led to the concentration of huge amounts of ilmenite. Complex variations in ilmenite composition in drill-cores depth profiles are reported that give evidence of the roles of fractional crystallization, multiple pulses of undifferentiated melts and magma mixing. By analogy with models proposed for the formation of chromitite (Irvine, 1975, 1977), the possible crystallization of ilmenite as the sole liquidus minerals is discussed. Finally, following a recent estimate of the cooling rate of the Havre-Saint-Pierre anorthosite and associated rocks (Morisset

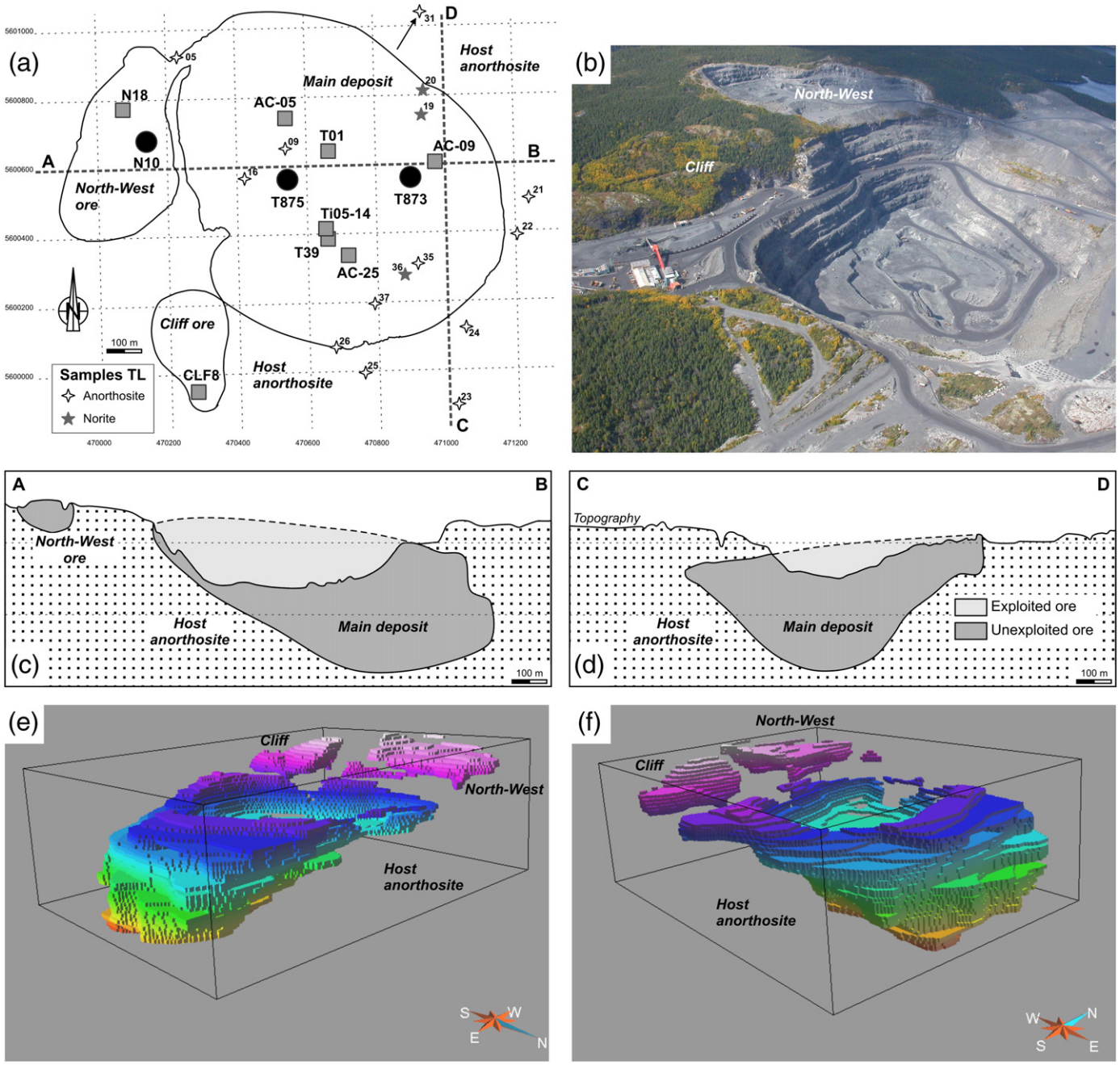

Fig. 3. Detailed views of the Allard Lake deposit. (a) Surface outline of the open-pit with location of rock samples (stars) and of drill-cores (black circles are drill-cores sampled for plagioclase and ilmenite separation and grey squares are mining drill-cores with whole-rock analyses; coordinates are UTM — Nad 83, Zone 20N). Heavy dashed lines indicate the position of the two cross sections (A–B and C–D); (b) Aerial picture of the deposit showing the open-pit in 2008; (c–d) West–East (A–B) and South–North (C–D) cross sections in the deposit showing the reconstructed exploited ore; (e–f) 3D shape of the deposit using 172,643 samples (GOCAD software). Colour scale is for the depth.

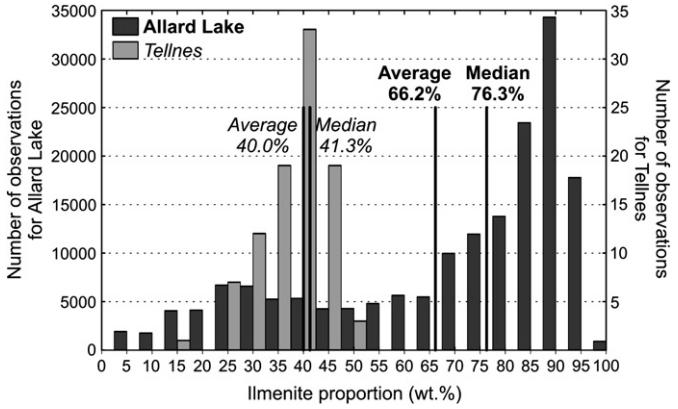

Fig. 4. Histograms of the ilmenite proportion in the Allard Lake ilmenite deposit ($n = 172{,}643$) compared to that in the Tellnes deposit ($n = 94$; data from Charlier et al., 2006).

et al., 2009), we describe postcumulus processes related to a metamorphic overprint that substantially modified primary igneous textures and mineral compositions.

2. Geological setting

The Havre-Saint-Pierre anorthosite complex is part of the late-Mesoproterozoic Grenville Province of North America that covers 1600×350 km along the southeastern margin of the Canadian Shield (e.g. Davidson, 1995, 2008). Rivers et al. (1989) have divided the Grenville Province into three orogen-parallel belts: the parautochtonous belt, the allochthonous polycyclic belt and the allochthonous monocyclic belt. These three belts are limited by two principal boundaries, namely the Grenville Front and the Allochton Boundary Thrust (Fig. 1). The allochthonous belts have also been grouped into different tectonic units on the basis of their Ottawan (1080–1020 Ma; Rivers, 1997) metamorphic signatures (Rivers, 2008). The allochthonous polycyclic belt contains many AMCG suites which have been emplaced in three different pulses at around 1160–1140 Ma, 1082–1050 Ma and 1020–1010 Ma (Higgins and van Breemen, 1996; Corrigan and van Breemen, 1997). The Grenvillian orogenic belt of Laurentia is correlated with the Sveconorwegian orogenic belt of the Baltic shield (Rivers et al., 1989; Romer, 1996; Rivers and Corrigan, 2000).

The composite Havre-Saint-Pierre anorthosite crops out along the northern shore of the Saint Lawrence estuary. It covers an area of 20,000 km² and is made up of several anorthositic plutons separated by monzonitic, mangeritic to granitic envelopes (Fig. 2; Wodicka et al., 2003). The Allard anorthosite, into which the ilmenite deposit was emplaced, has been dated at ca. 1061 Ma (U–Pb on zircon; Morisset et al., 2009), which is the same age as that of the smaller neighbouring Rivière au Tonnerre anorthosite, dated at 1062 ± 4 Ma (U–Pb on zircon; van Breemen and Higgins, 1993). These ages are coeval with the second stage of metamorphism during the Ottawan orogeny (1080–1020 Ma; Rivers, 1997; Rivers et al., 2002; Rivers, 2008). Dating of the mangeritic envelope of the Allard anorthosite from the Magpie river area gives an older age of $1126 + 7/-6$ Ma (U–Pb on zircon; Emslie and Hunt, 1990). The Havre-Saint-Pierre complex is commonly correlated with other anorthositic suites of Chateau-Richer, St-Urbain, Mattawa and Labrieville (Fig. 1; Owens et al., 1994; Owens and Dymek, 2001, 2005; Morisset et al., 2009). Jotunites (orthopyroxene monzodiorites), also called ferrodiorites or ferrobasalts, have been found as marginal units to anorthosite and as fine-grained dykes in these latter anorthosite suites (Owens et al., 1993; Icenhower et al., 1998). These

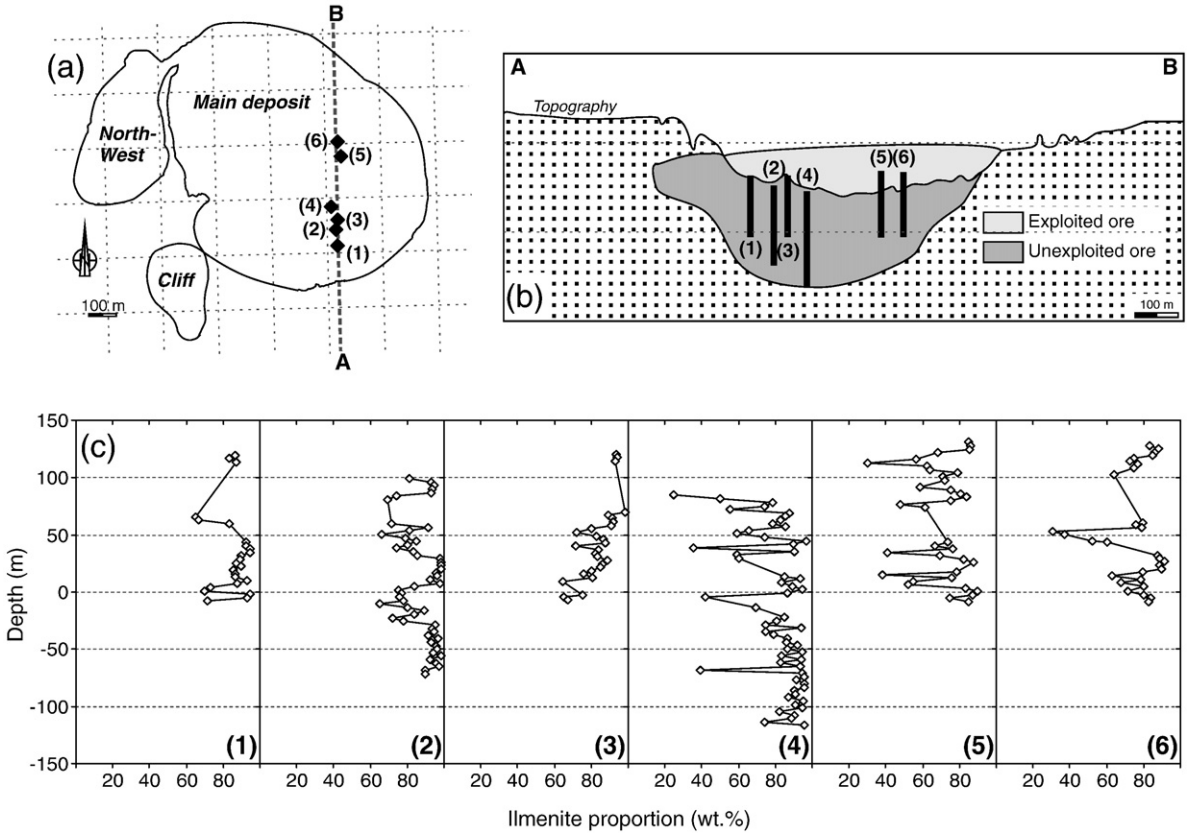

Fig. 5. Stratigraphic variation of ilmenite proportion in six selected drill-cores. (a) Surface outline of the open-pit with location of the six selected drill-cores and the South–North A–B cross section; (b) South–North (A–B) cross section in the deposit showing the position of the six drill-cores; (c) Stratigraphic variation of ilmenite proportion (wt.%) in holes 1 to 6.

liquid compositions display Fe-, Ti- and P-enrichment and intermediate Mg#.

The Allard massif-type anorthosite displays a domical structure and is surrounded by a continuous jotunitic to mangeritic margin, 1–10 km wide (Hocq, 1982). Rocks display petrographic evidence of ductile deformation (undulatory extinction in plagioclase) and dynamic recrystallization. Lithologies are essentially coarse-grained andesine anorthosite with plagioclase An_{37-49}, Or_{3-7}, 1000–1200 ppm Sr and 200–500 ppm Ba (Hargraves, 1962; Dymek, 2001) and less than 5% of orthopyroxene, ilmenite ± clinopyroxene. The rocks are generally equigranular (ca. 5 mm–2 cm) but some contain large plagioclase megacrysts 20 cm long. Norite and leuconorite constitute less than 1% of the outcrops and occur as sheets and layers of oxide-rich (gabbro-)norite (Hargraves, 1962). Enclaves of labradoritic anorthosite (An_{66-74}, 350–550 ppm Sr, <50–100 ppm Ba) occur in the western part of the anorthosite (Hocq, 1982; Dymek, 2001). All these characteristics together with the local occurrence of high-alumina orthopyroxene are typical features of massif-type anorthosite formed from polybaric crystallization (Emslie, 1985; Charlier et al., submitted for publication).

3. Sampling and analytical methods

An extensive mining database of 172,643 samples from 236 drill-cores provided by QIT-Fer et Titane Inc. has been used to draw the morphology of the deposit. The density (g/cm^3) of these samples has

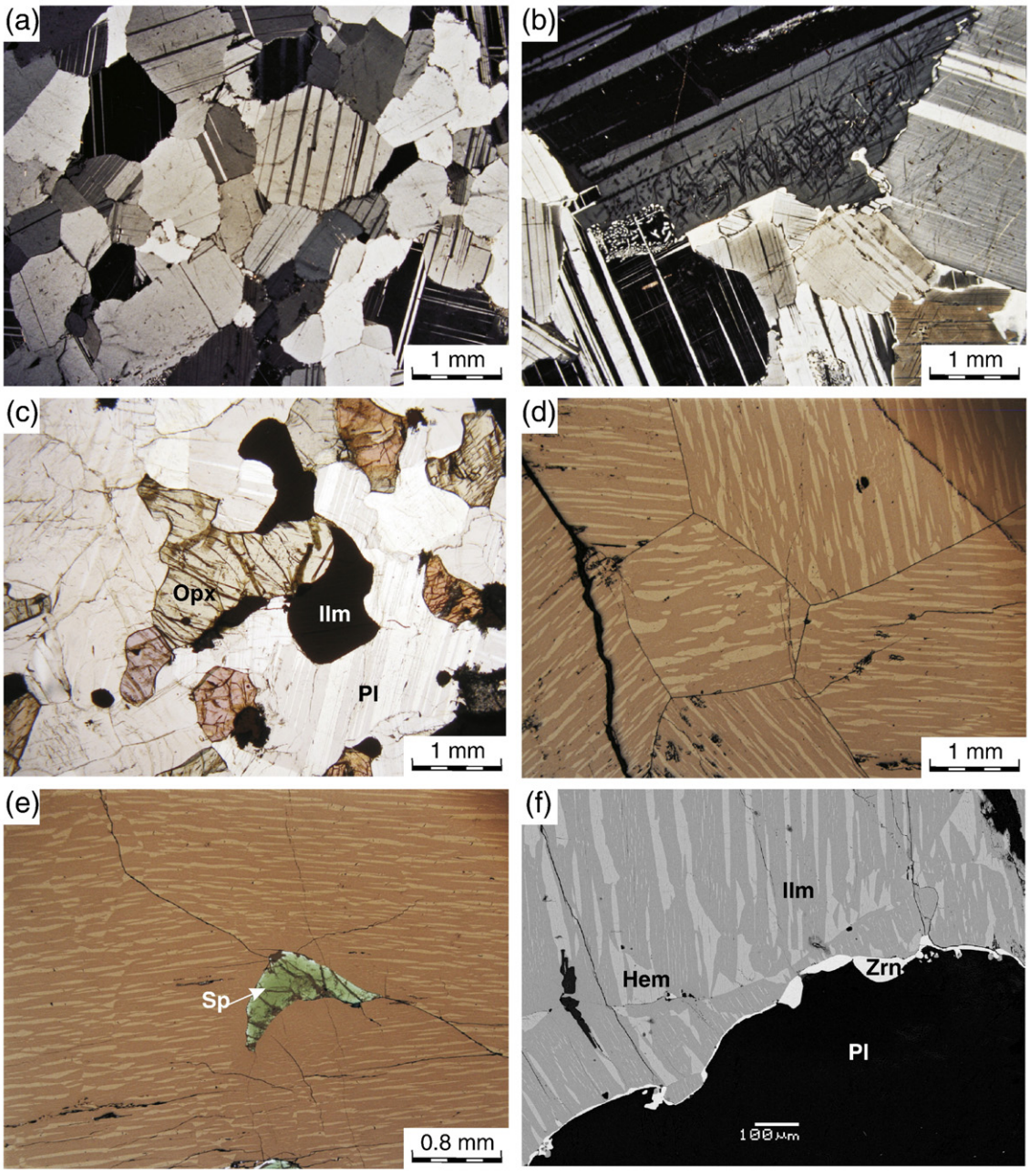

Fig. 6. Photomicrographs of the main rock types and ilmenite textures in the Allard Lake deposit. (a) Typical anorthosite with statically recrystallized plagioclase displaying 120° triple junctions (cross-polarized transmitted light, N10-152); (b) Moderately recrystallized anorthosite showing abundant exsolved orthoclase enclosed in the margin of plagioclases and interstitial quartz (cross-polarized transmitted light, T875-297); (c) Norite (transmitted light, T875-66); (d) Ilmenitite with polygonal ilmenite grains (reflected light, T873-178); (e) Small aluminous spinel granule in hemo-ilmenite; note the decreasing amount of hematite lamellae close to spinel (reflected and transmitted light, T873-224); (f) Hemo-ilmenite grain in contact with plagioclase, with a zircon rim (backscattered electron image, T873-219). Abbreviations: Pl = plagioclase, Ilm = ilmenite, Hem = hematite, Opx = orthopyroxene, Sp = aluminous spinel, Zrn = zircon.

been determined by weighing the dry sample in air and then in water. Of these samples, 3922 rocks have been analysed for whole-rock major and some trace elements composition by the mining company using XRF. Each sample is generally a 3 m portion of a split drill core but a few samples are shorter sections (1–2 m). Some cores have been selected for detailed description. New samples were also collected along 3 cores (labelled T873; T875 and N10) and fifteen samples were collected in the open-pit (Fig. 3).

Ilmenite (60–150 μm), separated using heavy liquids (bromoform and Clerici's solution) and a Frantz isodynamic magnetic separator, were analysed for major elements (Si, Ti, Al, Fe, Mn, Mg) by XRF on lithium–borate fused glass, and for trace elements (V, Cr, Zn, Zr, Nb) on pressed powder pellets following the method of Duchesne and Bologne (2009). Plagioclase (60–150 μm), separated by flotation in bromoform and magnetic separation, were analysed for major elements by XRF on lithium–borate fused glass and for Sr and Ba by XRF on pressed powder pellets.

Electron microprobe analyses of pyroxenes, sapphirine and aluminous spinel were performed using a CAMECA SX50 at Bochum University (Germany). An accelerating voltage of 15 kV and a beam current of 15 nA were used. Chemical analyses were corrected with ZAF software. The following standards were used: pyrope for Mg and Al; andradite for Si, Fe and Ca; spessartine for Al and Mn; rutile for Ti; jadeite for Na; ZnO for Zn; Cr_2O_3 for Cr and V metal for V.

4. Morphology and petrography of the deposit

The Allard Lake ore body may be subdivided into three separate parts (Fig. 3), namely the Main, Cliff and North–West deposits. The main deposit has an oval outcrop measuring 1100 × 1030 m. The thickness ranges from 100 to 300 m and the ore body dips 10–15° to the east. The eastern margin as well as the northern and the southern are relatively steep, giving the morphology of a funnel-shaped intrusion. The internal structure of the ore body, shown by marker horizons such as anorthosite layers, is globally parallel to the contact with the host anorthosite (Fig. 3c–d). The remaining tonnage is estimated at 125 Mt with an estimated 120 Mt already mined. The Cliff ore body has an ellipsoidal shape in map view and lies along the west side of the main body from which it is separated by a screen of anorthosite. The basal contact of the ore body with the host anorthosite is sharp and undulating. The Cliff ore reserves are estimated at 8.4 Mt. The North–West ore body is a 60 to 100 m-thick layer, containing 5 Mt of reserves.

The ore is a coarse-grained (5–20 mm) ilmenite-rich norite or ilmenitite, essentially made up of tabular crystals of hemo-ilmenite (66.2 wt.% on average) and plagioclase. Histograms of the proportion of ilmenite show that 50% of the samples contain more than 76.3 wt.% ilmenite (Fig. 4). This is much more than the Tellnes ilmenite deposit that contains 40 wt.% ilmenite on average (Charlier et al., 2006). The proportion of ilmenite in the Allard deposit varies abruptly with depth and ores with >75 wt.% ilmenite alternate with more leucocratic rocks (Fig. 5). As illustrated in the A–B cross section of Fig. 5, variations of ilmenite proportions in drill-cores are impossible to correlate laterally. These variations are thus interpreted to occur as lenses with extension smaller than 50 m.

Typical accessory minerals include aluminous spinel, orthopyroxene and Ti-phlogopite. Minor amounts of disseminated interstitial sulfides (pyrite, pyrrhotite, chalcopyrite, millerite and Co–Ni sulfides) are present. Primary magnetite is lacking; the most common magnetite is secondary in origin and together with rutile and anatase results from

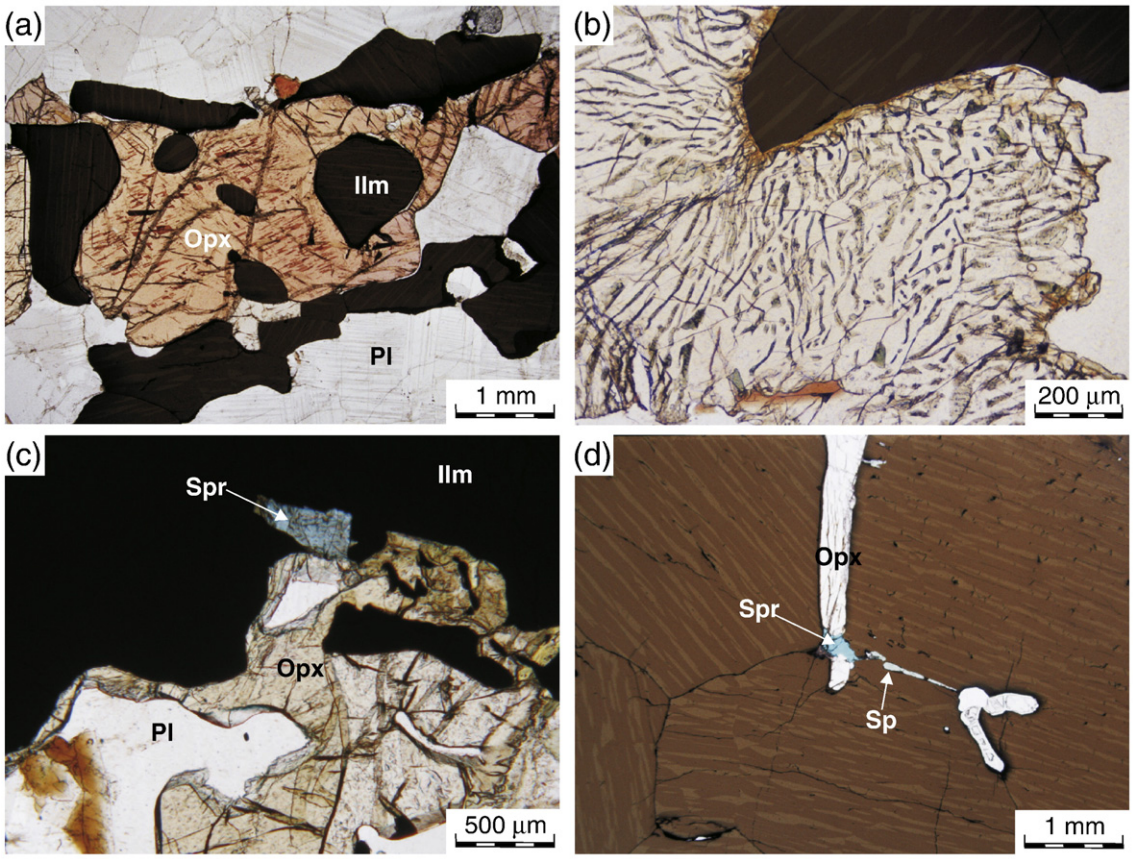

Fig. 7. Photomicrographs of the main textures of orthopyroxene and sapphirine in the Allard Lake ilmenite deposit. (a) Orthopyroxene with Schiller-type exsolved lamellae and included grains of hemo-ilmenite (transmitted light, T873-133); (b) Symplectitic intergrowth of high-alumina orthopyroxene and vermicular aluminous spinel (reflected and transmitted light, T873-291); (c) Small sapphirine grain at the contact between hemo-ilmenite and orthopyroxene (transmitted light, T873-268); (d) Sapphirine grain at the junction between orthopyroxene and aluminous spinel (reflected and transmitted lights, T873-68). Same abbreviations as in Fig. 6; Spr = sapphirine.

late-stage alteration of hemo-ilmenite. Calcite and gypsum occur locally in veinlets as alteration products.

Several groups of rocks have been distinguished among the samples based on the presence and relative proportions of plagioclase, ilmenite and orthopyroxene: anorthosite (>90% plagioclase; Fig. 6a–b), ilmenite–norite (<90% plagioclase, ilmenite), norite (<90% plagioclase, ilmenite, >2% orthopyroxene; Fig. 6c), opx–ilmenitite (>70% ilmenite, plagioclase, >2% orthopyroxene) and ilmenitite (>70% ilmenite, plagioclase; Fig. 6d). Two types of anorthosite occur: the host Havre-Saint-Pierre anorthosite and anorthositic layers and lenticular pods in the massive ore. Both types are petrographically very similar and only distinguished by their location. Norites occur in association with both types of anorthosite.

In the Allard deposit, ilmenite grains display 120° triple junctions (Fig. 6d) typical of an annealing texture resulting from static recrystallization. They contain less than 50% exsolved hematite and are thus referred to as hemo-ilmenite (Fig. 6e). Exsolved hematite commonly displays a preferred orientation in adjacent grains, implying that the lattice of the ilmenite had a similar orientation before the exsolution process. Twinning in ilmenite and equant ilmenite grains included in plagioclase are locally observed. Ilmenite may be rimmed against plagioclase by zircon (Fig. 6f; Morisset and Scoates, 2008) and baddeleyite locally occurs as small euhedral grains included in ilmenite. Hemo-ilmenite microstructures and the implications for their magnetic properties are detailed in McEnroe et al. (2007).

Grains of aluminous spinel are present at the margin of ilmenite crystals and are interpreted as due to external granule exsolution. Aluminous spinel also occurs as exsolved lenses or granules in ilmenite. A noticeable decrease in the amount of hematite lamellae in ilmenite is observed close to the exsolved aluminous spinel (Fig. 6e).

Prismatic orthopyroxene (1–4 mm) occurs in a few samples. It commonly contains Schiller lamellae (of hemo-ilmenite) and may include ilmenite grains (Fig. 7a). Rare symplectitic intergrowths of orthopyroxene and aluminous spinel have been detected (Fig. 7b).

Table 1
XRF analyses of separated ilmenite from the Allard Lake ilmenite deposit.

Sample	Ilm prop	TiO_2	Al_2O_3	Fe_2O_{3tot}	Fe_2O_3	FeO	MgO	Total	Xgeik	Xpyr	Xhem	Xilm	V	Cr	Zn	Mn	Zr	Nb
T873-50	91	37.81	1.26	61.58	29.57	28.80	2.83	100.27	0.105	0.003	0.276	0.616	1924	1036	122	1189	274	31
T873-60	94	37.73	1.34	61.61	29.28	29.09	2.63	100.07	0.098	0.003	0.274	0.625	1963	924	139	1162	776	21
T873-68	95	37.48	0.72	60.77	28.91	28.67	2.74	98.52	0.103	0.003	0.275	0.618	1895	883	90	1152	243	26
T873-79	92	37.28	1.29	61.84	30.64	28.08	2.97	100.26	0.110	0.003	0.286	0.601	2043	763	132	1159	195	33
T873-88	91	36.64	1.68	62.36	31.58	27.70	2.86	100.46	0.105	0.003	0.294	0.597	1859	829	194	1168	659	32
T873-98	86	36.77	1.45	61.99	30.64	28.21	2.64	99.71	0.098	0.003	0.288	0.611	1975	970	134	1177	183	33
T873-115	94	38.90	1.21	59.41	26.74	29.40	3.04	99.29	0.113	0.003	0.251	0.632	2282	2277	103	1206	281	27
T873-133	73	38.41	0.60	61.52	28.16	30.01	2.44	99.62	0.091	0.004	0.266	0.639	2136	2025	85	1352	24	29
T873-146	64	36.92	0.74	62.61	30.48	28.91	2.32	99.37	0.087	0.003	0.289	0.621	1898	1320	60	1131	188	36
T873-178	94	37.20	1.34	61.93	29.95	28.77	2.54	99.80	0.095	0.003	0.282	0.621	1963	1093	148	1156	371	29
T873-186	71	38.93	0.83	60.62	27.21	30.06	2.69	99.72	0.100	0.003	0.256	0.641	2098	450	65	1190	66	29
T873-194	91	36.85	1.54	61.90	30.29	28.45	2.54	99.67	0.095	0.003	0.285	0.617	2004	937	130	1201	255	32
T873-202	87	38.08	0.45	61.92	28.91	29.71	2.46	99.61	0.092	0.003	0.273	0.631	2084	1321	28	1198	296	33
T873-210	96	37.28	1.38	61.85	30.07	28.59	2.68	100.00	0.099	0.003	0.282	0.616	1970	1099	132	1164	334	28
T873-219	87	37.32	1.59	61.27	29.49	28.59	2.70	99.69	0.100	0.003	0.277	0.620	2090	1110	134	1139	422	36
T873-230	94	37.40	1.66	60.74	29.22	28.36	2.87	99.51	0.107	0.003	0.274	0.616	1984	650	167	1178	214	28
T873-242	90	37.23	1.61	61.86	30.11	28.57	2.67	100.19	0.099	0.003	0.281	0.617	1901	858	155	1164	642	22
T873-249	95	36.74	1.62	61.71	30.76	27.85	2.83	99.80	0.105	0.003	0.288	0.604	1862	601	182	1120	771	33
T873-259	92	37.77	1.31	61.37	29.38	28.78	2.82	100.06	0.104	0.003	0.275	0.618	1986	615	132	1161	56	33
T873-268	57	40.29	0.92	59.17	23.97	31.67	2.46	99.31	0.092	0.004	0.226	0.678	2149	845	46	1321	23	34
T873-276	93	36.64	1.94	61.56	30.88	27.61	2.91	99.98	0.108	0.003	0.288	0.601	1870	1500	218	1150	636	30
T873-283	91	36.81	1.57	61.22	30.17	27.94	2.81	99.30	0.105	0.003	0.284	0.608	1912	1226	163	1143	1261	23
T873-291	86	37.17	1.15	60.38	28.55	28.64	2.60	98.11	0.098	0.003	0.273	0.625	1946	1246	106	1184	1016	26
T873-296	93	38.87	0.76	61.74	26.24	31.94	1.59	99.40	0.060	0.004	0.250	0.687	2216	572	94	1306	22	33
T873-301	88	37.13	1.95	61.19	29.43	28.58	2.62	99.71	0.097	0.003	0.276	0.624	1983	847	160	1111	469	31
T873-307	94	37.31	1.42	61.45	29.42	28.82	2.57	99.54	0.096	0.003	0.277	0.624	2020	1218	153	1168	978	24
T873-314	94	37.65	1.37	61.27	28.98	29.05	2.61	99.66	0.097	0.003	0.272	0.627	2050	1144	170	1179	246	27
T873-320	76	38.14	0.49	62.69	29.60	29.78	2.45	100.46	0.091	0.003	0.278	0.628	1948	778	35	1166	273	34
T875-4	93	37.81	1.17	61.25	29.22	28.82	2.82	99.84	0.105	0.003	0.274	0.618	1891	995	96	1143	139	29
T875-14	93	37.98	1.52	61.09	29.09	28.80	2.92	100.31	0.108	0.003	0.271	0.618	1916	918	134	1125	390	29
T875-25	93	37.21	1.74	61.53	30.33	28.08	2.93	100.29	0.108	0.003	0.282	0.606	1877	870	185	1236	457	36
T875-35	86	38.28	1.10	60.66	27.76	29.61	2.61	99.36	0.098	0.003	0.262	0.637	2211	883	111	1215	177	32
T875-45	96	37.16	1.29	62.30	30.96	28.20	2.84	100.45	0.105	0.003	0.289	0.603	1927	811	116	1126	307	29
T875-53	95	36.52	0.90	61.97	30.36	28.45	2.38	98.61	0.090	0.003	0.290	0.617	1793	904	91	1149	288	31
T875-63	95	37.26	1.36	61.89	30.31	28.42	2.77	100.12	0.103	0.003	0.284	0.611	1879	811	129	1170	554	30
T875-79	89	37.93	1.93	60.27	28.77	28.34	3.15	100.12	0.116	0.003	0.267	0.613	2034	693	185	1196	150	24
T875-87	95	37.49	0.96	62.13	30.12	28.81	2.67	100.05	0.099	0.003	0.283	0.615	2072	1192	91	1167	354	35
T875-96	86	38.02	1.59	60.01	27.68	29.09	2.77	99.15	0.103	0.003	0.261	0.632	2365	1743	138	1213	163	26
T875-105	91	37.58	1.65	61.17	29.55	28.45	2.91	100.14	0.108	0.003	0.276	0.614	2210	1076	133	1125	232	32
T875-116	79	38.64	0.43	59.79	26.32	30.12	2.51	98.02	0.095	0.003	0.253	0.649	2339	1072	30	1199	153	25
T875-124	93	37.22	0.91	62.17	29.80	29.13	2.35	99.41	0.088	0.003	0.282	0.627	1994	1032	101	1160	250	38
T875-131	90	38.13	1.22	60.88	27.96	29.63	2.52	99.46	0.094	0.004	0.264	0.639	1987	846	126	1373	436	31
T875-139	85	38.64	1.29	60.04	26.64	30.06	2.54	99.17	0.095	0.003	0.252	0.650	2131	939	104	1266	279	39
N10-15	79	38.83	0.82	59.95	26.59	30.02	2.67	98.93	0.100	0.003	0.252	0.645	1958	1517	70	1110	240	28
N10-24	91	38.08	1.51	60.62	28.51	28.90	2.92	99.92	0.108	0.003	0.266	0.622	2158	1649	147	1088	298	30
N10-33	91	38.80	1.53	59.04	26.80	29.01	3.22	99.36	0.120	0.003	0.251	0.626	2180	1710	123	1084	222	22
N10-42	84	37.76	0.86	61.56	28.55	29.70	2.30	99.17	0.086	0.003	0.271	0.639	1944	1553	69	1176	525	33
N10-52	91	37.75	1.32	61.46	29.23	29.00	2.69	99.99	0.100	0.003	0.274	0.623	1984	1099	120	1137	369	27
N10-60	90	37.58	1.35	61.48	29.36	28.90	2.66	99.85	0.099	0.003	0.275	0.622	1925	1012	113	1171	375	36
N10-67	93	37.91	1.53	61.49	28.99	29.24	2.63	100.30	0.097	0.003	0.271	0.629	2210	1540	148	1208	483	27

Major elements in weight percent, FeO and Fe2O3 recalculated from $Fe2O3_{tot}$ by charge balance; molar fractions of geikielite (MgTiO3), pyrophanite (MnTiO3), hematite (Fe2O3) and ilmenite (FeTiO3) (Xgeik, Xpyr, Xhem, Xilm) calculated following QUILF algorithm (Andersen et al., 1993); trace elements in parts per million (ppm).

Sapphirine has been observed in five of a hundred thin sections (Fig. 7c–d) and is usually in contact with orthopyroxene and aluminous spinel. Clinopyroxene, locally containing cores of orthopyroxene, is present in the host anorthosite.

5. Mineral chemistry

5.1. Ilmenite

Separated ilmenites have been analysed for major and some trace elements (Table 1). The hematite content varies between $Hem_{22.6}$ and $Hem_{29.4}$. Cr ranges from 450 to 2277 ppm and has a poor positive correlation with V (1793–2365 ppm) (see Fig. 15). MgO (1.59–3.22 wt.%) is positively correlated with Al_2O_3 (0.36–1.95 wt.%) and Zn (27–218 ppm). This is interpreted to result from variable amounts of spinel in ilmenite and/or the loss of spinel during mineral separation. Zr in ilmenite spans a large range from 22 to 1261 ppm. This is most probably related to the amount of zircon exsolved from ilmenite.

Ilmenite compositions display irregular patterns in drill-cores (Fig. 8). The trends in each drill-cores are characterized by abrupt changes for all the elements. Both normal trends (decreasing contents of compatible elements with decreasing depth) and reverse trends (increasing contents of compatible elements with decreasing depth) are observed.

5.2. Plagioclase

The plagioclase in the Allard Lake ilmenite deposit and in the surrounding Allard anorthosite is generally andesine (Fig. 9; Table 2). Plagioclase compositions in norites and ilmenitites of the deposit vary from $An_{50.6}$ to $An_{41.7}$ and $Or_{0.4}$ to $Or_{6.5}$. Sr varies from 851 to 1518 ppm and Ba from 101 to 461 ppm. These are close to the plagioclase composition in the host Allard anorthosite: $An_{49.0–45.4}$, $Or_{3.6–6.3}$, Sr 962–1212 ppm and Ba 196–437 ppm. Moreover, anorthositic rocks within the Allard deposit display a similar range: $An_{51.0–43.7}$, $Or_{4.4–7.1}$, Sr 986–1165 ppm and Ba 194–398 ppm, and thus cannot be distinguished from plagioclase of the host Allard anorthosite.

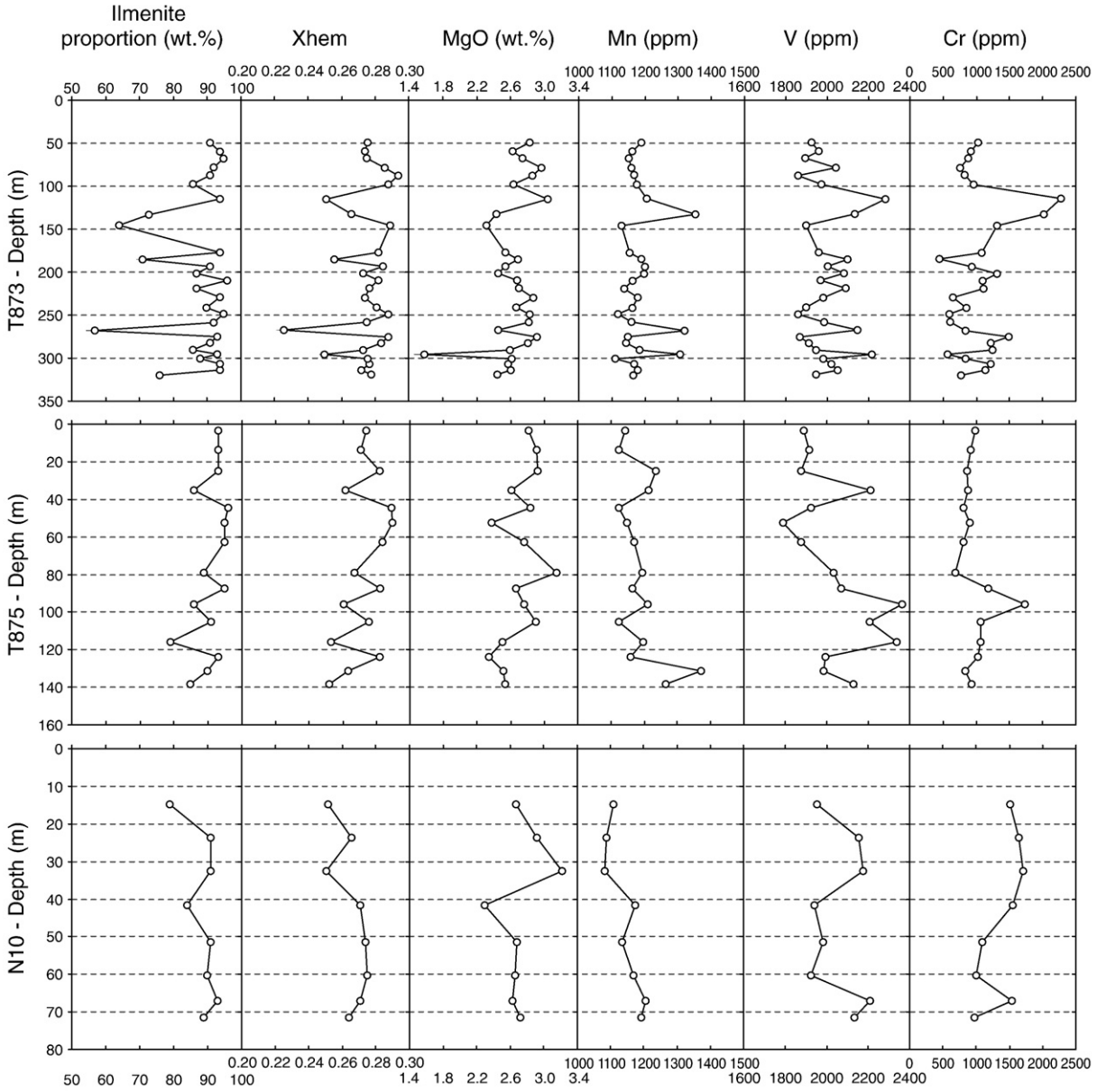

Fig. 8. Stratigraphic variation of ilmenite composition and ilmenite proportion in holes T873, T875 and N10 (see location on Fig. 3).

Table 2
Major and trace element compositions of separated plagioclase from the Allard Lake ilmenite deposit and the host Havre-Saint-Pierre anorthosite (XRF analyses).

Sample	Ilm prop	Rock type	SiO_2	TiO_2	Al_2O_3	Fe_2O_3	CaO	Na_2O	K_2O	Total	An	Or	Ba	Sr
T873-16	33	opx–norite	56.27	0.06	26.89	0.31	9.33	5.32	0.92	99.30	49.2	5.5	402	1176
T873-31	44	norite	56.19	0.08	26.77	0.41	9.09	5.21	1.08	99.13	49.1	6.5	409	1161
T873-50	91	ilmenitite	55.41	0.09	26.78	0.45	10.19	5.83	0.20	99.40	49.1	1.1	286	1138
T873-79	92	ilmenitite	56.57	0.15	26.37	0.63	8.60	6.40	0.26	99.81	42.6	1.5		
T873-99	86	ilmenitite	56.10	0.11	26.99	0.60	9.18	5.92	0.26	99.71	46.1	1.5	283	1131
T873-101	17	opx–norite	56.38	0.06	26.81	0.40	9.29	5.24	0.79	99.23	49.5	4.8	341	1135
T873-125	8	opx–norite	56.98	0.06	26.73	0.34	9.03	5.33	1.02	99.66	48.4	6.1	461	1331
T873-133	73	opx–ilmenitite	56.06	0.10	26.99	0.38	9.31	5.47	0.45	99.14	48.5	2.7	336	1518
T873-146	64	norite	56.37	0.09	27.02	0.27	9.27	5.26	0.84	99.39	49.3	5.1	394	1193
T873-157	6	deposit anorthosite	56.79	0.06	26.11	0.70	8.98	5.41	1.04	99.64	47.8	6.2	275	1111
T873-166	5	deposit anorthosite	56.90	0.06	26.61	0.41	9.02	5.37	0.84	99.39	48.1	5.1	367	1125
T873-186	71	ilmenitite	55.90	0.10	27.18	0.32	9.49	5.30	0.67	99.12	49.7	4.0	319	1201
T873-190	5	deposit anorthosite	56.69	0.08	26.57	0.39	9.20	5.16	0.94	99.15	49.6	5.7	398	1165
T873-194	91	ilmenitite	56.39	0.13	27.15	0.37	9.31	5.87	0.22	99.71	46.7	1.3	331	1181
T873-202	87	ilmenitite	56.08	0.10	27.13	0.36	9.23	5.87	0.19	99.22	46.5	1.1	307	1324
T873-220	87	ilmenitite	56.02	0.10	27.00	0.33	9.21	5.81	0.19	98.99	46.7	1.1	313	1291
T873-242	90	ilmenitite	55.99	0.12	26.98	0.37	9.36	5.93	0.14	99.17	46.6	0.8		
T873-259	92	ilmenitite	56.02	0.14	26.81	0.42	9.77	5.96	0.14	99.56	47.5	0.8		
T873-268	57	opx–norite	55.89	0.10	27.46	0.25	9.59	5.65	0.25	99.40	48.4	1.5	270	1264
T873-283	91	ilmenitite	56.14	0.14	26.90	0.41	9.24	6.06	0.07	99.20	45.7	0.4		
T873-291	86	opx–ilmenitite	56.67	0.10	27.15	0.36	9.20	5.97	0.08	99.67	46.0	0.5		
T873-296	93	ilmenitite	56.24	0.11	27.11	0.35	9.63	5.93	0.07	99.80	47.3	0.4		
T873-301	88	opx–ilmenitite	56.20	0.10	27.30	0.37	9.43	5.86	0.06	99.49	47.1	0.4	246	1366
T873-316	3	deposit anorthosite	56.45	0.04	26.84	0.29	8.52	5.43	1.04	98.91	46.4	6.3	194	1148
T873-320	76	opx–ilmenitite	57.00	0.06	26.71	0.32	8.75	6.01	0.31	99.36	44.6	1.8	198	1163
T873-321	38	opx–norite	57.96	0.05	25.74	0.55	8.11	5.93	0.52	99.15	43.0	3.2	101	1056
T873-322	4	host anorthosite	56.74	0.03	26.83	0.22	9.09	5.58	0.78	99.30	47.4	4.6	246	1139
T875-25	93	ilmenitite	57.16	0.11	25.73	0.55	8.33	6.44	0.18	99.27	41.7	1.1		
T875-35	86	ilmenitite	56.28	0.10	27.17	0.26	9.25	5.88	0.17	99.45	46.5	1.0	278	1204
T875-66	16	norite	56.90	0.07	26.92	0.29	9.28	5.25	0.83	99.62	49.4	5.0	346	1203
T875-79	89	ilmenitite	56.48	0.12	27.03	0.48	9.17	6.02	0.13	99.61	45.7	0.8	234	851
T875-91	0	deposit anorthosite	56.89	0.07	26.74	0.40	9.33	4.95	1.01	99.52	51.0	6.2	386	1151
T875-96	86	ilmenitite	56.02	0.09	27.52	0.36	9.67	5.68	0.19	99.87	48.5	1.1	181	1174
T875-106	91	ilmenitite	56.02	0.12	27.22	0.38	9.45	5.81	0.09	99.44	47.3	0.5	184	1184
T875-116	79	ilmenitite	56.40	0.08	27.05	0.32	9.35	5.64	0.38	99.39	47.8	2.3	251	1045
T875-140	0	host anorthosite	56.91	0.04	26.63	0.46	8.52	5.67	0.95	99.54	45.4	5.7	437	1026
T875-150	0	host anorthosite	57.01	0.03	26.61	0.30	8.69	5.67	0.89	99.33	45.9	5.3	284	1000
T875-165	0	host anorthosite	57.30	0.03	26.63	0.28	8.70	5.67	1.04	99.76	45.9	6.1	315	1135
N10-6	88	ilmenitite	55.47	0.12	27.33	0.36	9.66	5.52	0.27	99.08	49.2	1.6	300	1280
N10-15	79	ilmenitite	55.69	0.11	27.66	0.32	9.84	5.30	0.43	99.60	50.6	2.6	280	1293
N10-24	91	ilmenitite	55.87	0.11	27.35	0.31	9.67	5.62	0.25	99.46	48.7	1.5	283	1262
N10-33	91	ilmenitite	55.51	0.13	27.20	0.39	10.09	5.78	0.13	99.55	49.1	0.7	276	1177
N10-42	84	ilmenitite	55.77	0.12	27.02	0.48	9.54	5.78	0.27	99.39	47.7	1.6		
N10-52	91	ilmenitite	55.62	0.12	27.07	0.31	9.69	5.78	0.14	99.01	48.1	0.8	250	1187
N10-54	2	deposit anorthosite	56.97	0.09	26.74	0.54	8.10	5.76	0.97	99.62	43.7	5.9	310	1124
N10-60	90	ilmenitite	55.08	0.12	26.77	0.53	10.14	5.84	0.21	99.11	49.0	1.2		
N10-67	93	ilmenitite	55.72	0.11	26.75	0.34	9.88	5.98	0.13	99.31	47.7	0.7	220	1301
N10-72	89	ilmenitite	56.46	0.10	27.36	0.28	9.48	5.84	0.11	99.97	47.3	0.6	269	1255
N10-75	0	host anorthosite	56.76	0.05	26.76	0.31	9.51	5.68	0.77	99.94	48.1	4.4	250	1212
N10-106	0	host anorthosite	55.90	0.03	26.42	0.24	10.01	5.76	0.65	99.07	49.0	3.6	213	1164
N10-152	0	host anorthosite	56.81	0.03	26.79	0.24	9.41	5.57	0.63	99.53	48.3	3.7	237	1055
TL05	0	host anorthosite	56.39	0.04	26.89	0.33	9.16	5.57	0.72	99.14	47.6	4.3	244	1181
TL09	0	deposit anorthosite	56.70	0.04	26.62	0.38	8.62	5.44	1.18	99.28	46.7	7.1	262	986
TL16	0	host anorthosite	56.58	0.05	26.66	0.39	8.75	5.58	1.06	99.28	46.4	6.3	298	1167
TL19	5	opx–norite	56.30	0.05	27.02	0.51	9.43	5.29	0.84	99.60	49.6	5.0	348	1060
TL20	2	opx–norite	56.15	0.05	26.94	0.53	9.26	5.29	0.93	99.43	49.2	5.6	377	1000
TL21	0	host anorthosite	56.42	0.05	26.78	0.23	9.41	5.59	0.66	99.18	48.2	3.9	213	962
TL22	0	host anorthosite	56.58	0.03	26.90	0.31	9.20	5.54	0.70	99.33	47.9	4.2	235	1083
TL23	0	host anorthosite	56.76	0.03	27.03	0.25	9.32	5.52	0.62	99.59	48.3	3.7	206	1027
TL24	0	host anorthosite	56.94	0.03	26.78	0.24	9.14	5.55	0.67	99.41	47.6	4.0	196	1121
TL25	0	host anorthosite	56.82	0.03	26.70	0.27	9.13	5.62	0.64	99.26	47.3	3.8	272	1055
TL26	0	host anorthosite	56.90	0.03	26.87	0.27	9.01	5.65	0.70	99.51	46.8	4.2	221	1098
TL31	0	host anorthosite	56.73	0.05	26.83	0.27	9.25	5.49	0.62	99.29	48.2	3.7	230	1182
TL35	10	deposit anorthosite	57.02	0.21	26.68	0.27	9.09	5.50	0.81	99.77	47.7	4.8	391	1142
TL36	4	opx–norite	56.57	0.04	26.84	0.38	9.15	5.56	0.78	99.61	47.6	4.6	335	1121
TL37	0	deposit anorthosite	56.92	0.07	26.45	0.30	8.93	5.56	0.74	99.06	47.0	4.4	287	1134

An = 100[Ca/(Ca + Na)]; Or = 100[K/(Ca + Na + K)]; Sr and Ba in ppm.

Histograms of the distribution of plagioclase composition for each petrographic type (Fig. 9) show that plagioclase in ilmenite-rich rocks has a significant lower Or content than plagioclase in anorthosite and norite.

5.3. Aluminous spinel

Average compositions for aluminous spinel have X_{spinel} from 0.564 to 0.628 (Table 3). The MnO content is low (0.05–0.06 wt.%)

Table 3
Microprobe analyses of aluminous spinel from the Allard Lake ilmenite deposit.

Sample	*n*	Ilm prop	Rock type	TiO_2	Al_2O_3	FeO	MgO	MnO	Cr_2O_3	ZnO	V_2O_3	Total	X_{herc}	X_{spinel}	X_{gal}	X_{gah}
T873-68	12	95	ilmenitite	0.01	62.87	16.67	17.10	0.06	0.71	1.48	0.05	98.94	0.344	0.628	0.001	0.027
T873-133	11	73	opx–ilmenitite	0.04	60.02	17.99	15.39	0.05	3.63	2.02	0.07	99.21	0.381	0.580	0.001	0.038
T873-268	11	57	opx–norite	0.04	61.42	20.07	15.44	0.06	0.92	1.26	0.07	99.28	0.412	0.564	0.001	0.023
T873-291	14	86	opx–ilmenitite	0.02	62.59	18.52	15.83	0.06	0.88	1.14	0.06	99.10	0.387	0.590	0.001	0.021
T873-296	84	93	ilmenitite	0.04	62.07	18.57	16.32	0.06	1.05	1.12	0.06	99.29	0.381	0.597	0.001	0.020

X_{herc}, X_{spinel}, X_{gal} and X_{gah} are molar fractions of hercynite (FeAl2O4), spinel (MgAl2O4), galaxite (MnAl2O4) and gahnite (ZnAl2O4) respectively; *n* is the number of microprobe analyses.

while the ZnO content is relatively high, from 1.12 to 2.02 wt.% ($X_{gahnite}$ = 0.020–0.038). Detailed profiles across spinel grains reveal significant zonings (Fig. 10), particularly for Mg/Fe ratios and Cr_2O_3 content. Single grains have a higher $X_{hercynite}$ and lower Cr_2O_3 contents in the core and X_{spinel} and Cr_2O_3 enrichments towards the margin. ZnO is also higher at the margin while no systematic variations for the MnO content have been observed.

5.4. Pyroxenes

The composition of orthopyroxene ranges from $En_{75.7}$ to $En_{58.4}$ (Table 4). The Al_2O_3 content of orthopyroxene is from 1.48 to 9.08 wt.% and two types may be distinguished: low-alumina (1.48–3.09 wt.%) and high-Wo (0.6–1.5 mol%) orthopyroxenes on one hand and high-alumina (7.62–9.08 wt.%) and low-Wo (0.1–0.3 mol%) orthopyroxenes on the other hand (Fig. 11). The latter type of orthopyroxene occurs in samples in which sapphirine was detected. In contrast to high-alumina orthopyroxene megacrysts (Emslie, 1975; Longhi et al., 1993; Charlier et al., submitted for publication) interpreted to have crystallized under high pressure (11–13 kbar), Al-rich orthopyroxene from the Allard deposit does not contain exsolved plagioclase. MnO (0.17–0.84 wt.%) has a clear negative correlation with Mg#. The Mg# of clinopyroxene varies from 77.6 to 72.9 (Table 4).

5.5. Sapphirine

Sapphirine composition has been recalculated according to the scheme of Owen and Greenough (1991). The analysed sapphirines are markedly magnesian ($Mg/(Mg+Fe^{2+})$ = 0.83). The calculated $Fe^{3+}/(Fe^{2+}+Fe^{3+})$ ratios are 0.33–0.35. Cr_2O_3 has not been analysed but reach 0.50 wt.% in similar occurrences (Morisset et al., submitted for publication).

6. Whole-rock composition

Whole-rock analyses are plotted in major element binary diagrams (Fig. 12). TiO_2 and Al_2O_3 have been chosen as variation indexes, as they are related to the modal abundance of ilmenite and plagioclase, respectively. Compositional ranges of plagioclase, ilmenite and the two types of orthopyroxene are also plotted.

Whole-rock compositions display a large range: TiO_2 0.61–41.71 wt.%; Fe_2O_{3tot} 0–66.30 wt.%; Al_2O_3 0–26.23 wt.%; CaO 0–10.33 wt.%; and MgO 0.01–7.48 wt.%. It is obvious that bulk compositions are essentially controlled by the relative proportion of ilmenite and plagioclase as demonstrated by a linear distribution between ilmenite and plagioclase compositions in a TiO_2 vs. Al_2O_3 diagram (Fig. 12). When MgO is plotted as a function of Al_2O_3 or TiO_2, a minority of samples define a triangular field between the compositions of plagioclase, ilmenite and orthopyroxene. Anecdotally, some samples display a significant CaO-enrichment (CaO vs. Al_2O_3 diagram; Fig. 12) which is related to the presence of late calcite and gypsum veins in some rocks.

7. Discussion

7.1. Evidence for magma mixing

Because of the high value of $D_{Cr}^{Ilm/Liq}$ (e.g. Klemme et al., 2006), the Cr content of ilmenite is a good indicator of replenishment by primitive magma, since it should abruptly increase after a new injection of undifferentiated melt. Although major and trace element compositions of whole-rocks reflect the modal mineralogy of the samples, the Cr/TiO_2 ratio may be considered as a proxy for the Cr content of the ilmenite because Cr is exclusively contained in ilmenite and aluminous spinel that result from exsolution from ilmenite. Using the average TiO_2 content of ilmenite (37.71 ± 0.75 wt.%; Table 1), the Cr content of ilmenite (Cr_{ilm}) may be calculated from whole-rock composition (Cr_{WR}) using the equation:

$$Cr_{ilm} = Cr_{WR} * TiO_{2ilm} / TiO_{2WR}$$

Like the measured compositions of ilmenite (Fig. 8), the calculated Cr concentrations of ilmenite in 8 selected drill-cores display large variations (Fig. 13). Normal (decreasing Cr content) and reverse (increasing Cr content) trends alternate over distances less than 10 m thus displaying saw-tooth type of variation, which implies crystallization of ilmenite from continuously changing melt compositions as a result of three processes: (1) crystal fractionation (normal trends), (2) emplacement of new primitive magma and (3) progressive magma hybridisation. Even if the shifts to more primitive compositions are locally abrupt (for instance in core T01; Fig. 13), which suggest crystallization of ilmenite from a new undifferentiated melt composition, sequences of samples that become richer in Cr imply progressive hybridisation.

Stratigraphic and lateral variations of the Cr concentration in ilmenite are presented in the cross section of Fig. 14. Similarly to what has been observed for the ilmenite content in ore rocks, obvious lateral correlations cannot be found, even if the six presented drill-cores display similar saw-tooth variations. Consequently, we cannot conclude that such correlations do not exist as there are evidently occulted by complex small scale vertical variations.

The composition of liquids that are repeatedly injected in the deposit remains uncertain as no chilled margins, fine-grained rocks or dykes have been found in association with the Allard Lake ilmenite deposit. However, by analogy with the Tellnes ilmenite deposit that was also emplaced in an andesine massif-type anorthosite and contains plagioclase-ilmenite rocks (Charlier et al., 2006), it is most probable that the parental magma of the Allard Lake ilmenite deposit has also a ferrobasaltic composition. This is supported by the studies of Owens et al. (1993) and Icenhower et al. (1998) that described Fe-, Ti- and P-enriched liquids associated with some Grenvillian anorthosites such as St-Urbain and Labrieville.

7.2. Magma mixing and ilmenite stability

Magma mixing producing a hybrid located in the stability field of chromite has been proposed to explain the origin of chromitite layers

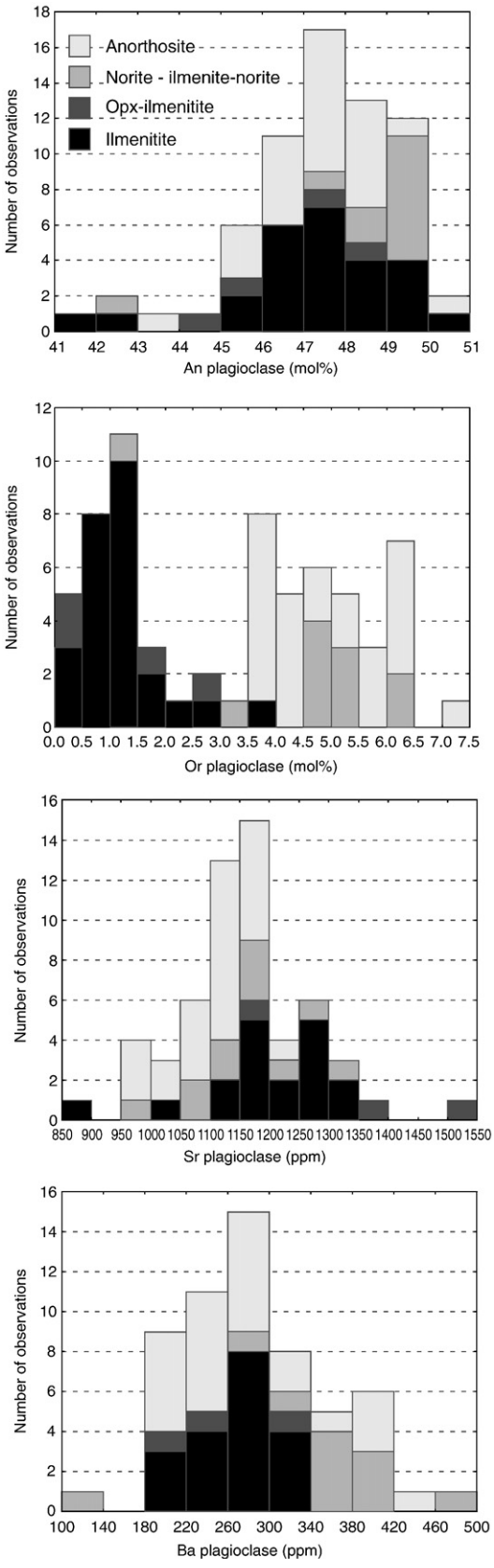

Fig. 9. Histograms of the composition of plagioclase for the contents of anorthite, orthoclase, Sr and Ba. Data for different rock types are stacked.

in magma chambers (Irvine, 1975, 1977). Mixing occurs either between the resident fractionated magma and a new, more primitive one, or by contamination of the resident magma by a siliceous component. This mechanism has been corroborated by many studies (e.g. Roeder and Reynolds, 1991; Campbell and Murck, 1993; Kinnaird et al., 2002) that have provided supporting evidence from mineral compositions, modal proportions, fluid dynamics, experimental studies and isotopic ratios.

Phase diagrams for plagioclase-ilmenite saturated liquids are poorly constrained. Nevertheless, plagioclase and ilmenite are known to crystallize as early liquidus phases in several intrusion: the Bjerkreim-Sokndal (SW Norway) and Grader layered intrusions (Wilson et al., 1996; Charlier et al., 2008) and the Tellnes ilmenite deposit (Charlier et al., 2006) are the best examples. Calculations of the cotectic proportions of ilmenite in ferrobasalts leads to values of 17.5 wt.% in the Tellnes ilmenite deposit (SW Norway; Charlier et al.,

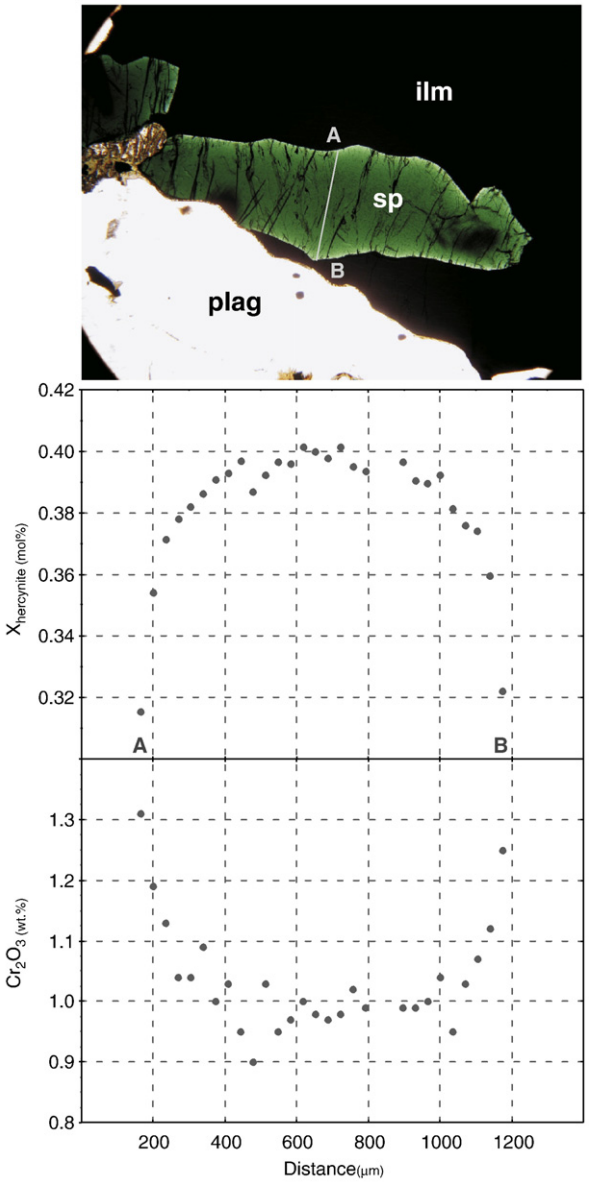

Fig. 10. Compositional profiles for $X_{hercynite}$ and Cr_2O_3 across aluminous spinel in sample T873-296. The distance scale is from an arbitrary starting point and only relative distances have any significance.

Table 4
Microprobe analyses of orthopyroxene, clinopyroxene and sapphirine from the Allard Lake ilmenite deposit and the host Havre-Saint-Pierre anorthosite.

Sample	*n*	Ilm prop	Rock type	SiO_2	TiO_2	Al_2O_3	FeO	MnO	MgO	CaO	Na_2O	Total	Mg#	En	Fs	Wo
Orthopyroxene																
T873-68	15	95	Ilmenitite	50.39	0.15	7.77	14.85	0.18	26.04	0.03	0.03	99.44	75.8	75.7	24.2	0.1
T873-101	22	17	Opx–norite	52.61	0.14	1.53	20.47	0.33	23.28	0.72	0.02	99.10	67.0	66.0	32.5	1.5
T873-125	21	8	Opx–norite	52.88	0.13	1.81	19.72	0.31	23.89	0.69	0.02	99.45	68.4	67.4	31.2	1.4
T873-133	14	73	Opx–ilmenitite	52.56	0.17	3.09	16.98	0.24	25.73	0.46	0.02	99.25	73.0	72.3	26.8	0.9
T873-190	21	5	Allard anorthosite	51.18	0.13	2.87	22.71	0.44	21.74	0.29	0.02	99.38	63.0	62.7	36.7	0.6
T873-268	10	57	Opx–norite	49.02	0.16	9.08	16.94	0.19	23.99	0.05	0.03	99.46	71.6	71.5	28.3	0.1
T873-291	17	86	Opx–ilmenitite	49.94	0.15	8.36	16.13	0.18	24.80	0.06	0.01	99.63	73.3	73.2	26.7	0.1
T873-296	20	93	Ilmenitite	49.82	0.18	8.46	15.33	0.17	25.45	0.09	0.02	99.52	74.7	74.6	25.2	0.2
T875-87	12	95	Ilmenitite	50.42	0.20	7.62	15.84	0.19	26.01	0.14	0.02	100.44	74.5	74.3	25.4	0.3
N10-75	10	0	Host anorthosite	53.01	0.14	1.50	21.12	0.59	23.40	0.57	0.01	100.34	66.4	65.6	33.2	1.1
TL19	13	5	Opx–norite	53.08	0.22	1.66	19.92	0.35	24.06	0.71	0.02	100.02	68.3	67.3	31.3	1.4
TL20	19	2	Opx–norite	52.60	0.17	1.48	21.16	0.39	22.98	0.59	0.02	99.39	65.9	65.1	33.7	1.2
TL31	10	0	Host anorthosite	51.61	0.21	1.54	24.83	0.84	20.14	0.54	0.02	99.73	59.1	58.4	40.4	1.1
TL36	25	4	Opx–norite	52.65	0.15	1.60	20.73	0.32	23.14	0.66	0.02	99.27	66.6	65.6	33.0	1.4
Clinopyroxene																
T873-166	21	5	Deposit anorthosite	50.80	0.58	2.81	8.71	0.20	13.22	22.55	0.47	99.34	73.0	38.5	14.2	47.2
N10-75	6	0	Host anorthosite	52.21	0.29	2.10	7.36	0.23	14.28	23.47	0.35	100.29	77.6	40.5	11.7	47.8
N10-152	10	0	Host anorthosite	51.72	0.33	2.30	8.51	0.33	13.27	22.98	0.47	99.91	73.5	38.4	13.8	47.8
TL20	12	2	Opx–norite	51.17	0.57	2.83	8.71	0.18	13.56	21.89	0.47	99.38	73.5	39.7	14.3	46.0
TL31	20	0	Host anorthosite	51.28	0.44	2.87	8.69	0.26	13.12	22.50	0.49	99.65	72.9	38.4	14.3	47.3
Sapphirine																
T873-68	4	95	Ilmenitite	12.70	0.06	59.68	9.17	0.07	16.14	0.01	0.01	97.89				
T873-268	18	57	Opx–norite	11.96	0.09	61.62	8.60	0.05	15.90	0.01	0.00	98.23				

Mg# = 100[Mg/(Mg + Fe)]; En = 100[Mg/(Mg + Fe + Ca)]; Fs = 100[Fe/(Mg + Fe + Ca)]; Wo = 100[Ca/(Mg + Fe + Ca)]; *n* is the number of microprobe analyses.

2007) and to 21 wt.% in the Grader layered intrusion (Charlier et al., 2008). These values, in accordance with experimental works on ferrobasalts (Toplis and Carroll, 1995), are low compared to the modal proportions observed in these two intrusions. However, the arguments against magma mixing in these two intrusions and in favour of continuous fractional crystallization are based on progressively changing cryptic variations exhibited by the cumulus minerals, that can be successfully modelled by simple Rayleigh fractionation. Thus, the invoked mechanism for ilmenite enrichment was flotation and removal of plagioclase.

In the Allard Lake deposit, even if ilmenite enrichment due to plagioclase flotation cannot be ruled out, it is evident that it cannot solely be associated with uninterrupted fractional crystallization. As previously discussed, magma mixing is evidenced by reverse cryptic variations in ilmenite (Figs. 13, 14). This is also shown in Fig. 15, where the evolution of Cr in ilmenite as a function of V does not display any clear evolutionary trend. Ilmenite compositions are spread between two differentiation trends: fractionation of pure ilmenite and of plagioclase and ilmenite in cotectic proportions. Two plausible cotectic fractions of ilmenite ($X_{ilm} = 0.21$ and 0.16) are displayed, consistent with the range of values calculated from natural and experimental data (Toplis and Carroll, 1995; Charlier et al., 2007, 2008). It is highly probable that the natural plagioclase-ilmenite cotectic is curved and that mixing of two magmas lying on the cotectic can produce a hybrid located in the stability field of ilmenite, that will crystallize alone until the liquid joins the cotectic and accumulate due to high density contrast with the liquid. However, the paucity of rocks with cotectic proportions of ilmenite and plagioclase (15–25 wt.% ilmenite and 85–75 wt.% plagioclase) leads us to suggest that the liquid did not follow the cotectic during significant periods of fractionation, in accordance with the multiple magma mixing events recorded by ilmenite compositions. Moreover, ilmenite enrichment might additionally result from plagioclase flotation, even if no direct evidence of plagioclase accumulation at the top of the intrusion has been observed. Plagioclase from the Allard Lake ilmenite deposit has the same composition than the plagioclase from host Havre-Saint-Pierre anorthosite. Thus the floated cumulates would be indistinguishable from the enclosing anorthosite.

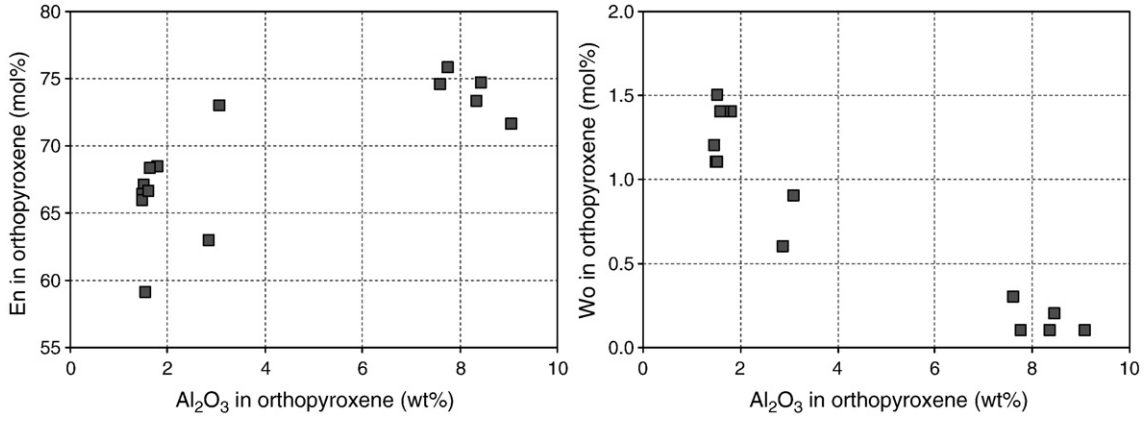

Fig. 11. Enstatite (100[Mg/(Mg + Fe + Ca)]) and Wollastonite (100[Ca/(Mg + Fe + Ca)]) as a function of Al_2O_3 in orthopyroxene.

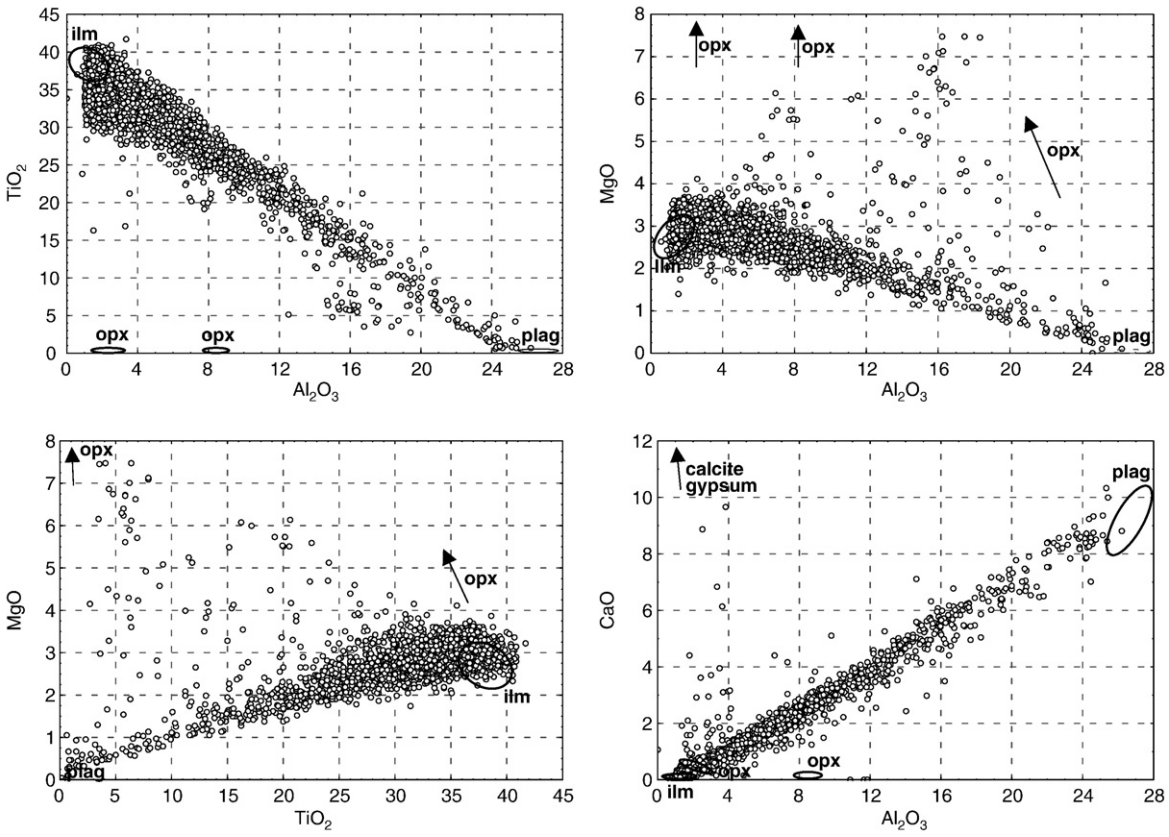

Fig. 12. Binary major elements variation diagrams of whole-rocks from the Allard Lake ilmenite deposit. The compositional ranges of main minerals are represented by an elliptic area or indicated by an arrow (plag = plagioclase, ilm = ilmenite, opx = orthopyroxene). Note that both high- and low-alumina orthopyroxenes are plotted.

7.3. Conduit or layered intrusion?

The Allard Lake deposit occurs as a large body of massive ilmenite, with minor norites. Some modal layering is present close to the margin with the host anorthosite, but these layers cannot be traced for significant distances. This contrasts with the Grader layered intrusion that displays continuous evolution of liquidus minerals and a sandwich horizon where the upper and lower solidification fronts met (Charlier et al., 2008).

The occurrence of multiple magma mixing events and the lack of lateral correlations over significant distances support the view that the Allard Lake deposit should not be regarded as a slowly cooled magma chamber but rather as a magma conduit in which density driven accumulation of ilmenite occurs. Moreover, compared to the 4–5 km diameter Grader layered intrusion, which is situated less than 2 km away from the Allard Lake mine, the latter only contains the first stage of evolution of a ferrobasaltic magma. The base of the Grader intrusion is similar to the Allard Lake deposit with a disturbed Cr evolution in ilmenite in its 25 m-thick basal massive ilmenite-rich portion (Charlier et al., 2008). There, ilmenite contains 800–900 ppm Cr and is more evolved than ilmenite in Allard Lake (ca. 2400 ppm Cr), but corresponds to the most common concentrations of Cr in the deposit (Fig. 16). However, the Grader layered intrusion contains more evolved cumulates with apatite, magnetite and clinopyroxene as liquidus phases, that are not present in the Allard Lake deposit.

A dynamic environment of emplacement has been documented for major Ni–Cu sulfide deposits such as Noril'sk, Jinchuan and Voisey's Bay (e.g. Li and Naldrett, 1999; Maier et al., 2001; De Waal et al., 2004; Li et al., 2004). In the Allard Lake deposit, the potential for ilmenite ore formation in a conduit system is enhanced by the injection of multiple pulses of undifferentiated magma that could crystallize large amounts of ilmenite. This mechanism also conveniently explains the absence of evolved cumulates and residual liquids.

7.4. Postcumulus processes and metamorphic overprint

The crystallization age of the Allard anorthosite has been dated to ca. 1061 Ma (U–Pb on zircon; Morisset et al., 2009), which is synchronous with the second stage of metamorphism during the Ottawan orogeny (1080–1020 Ma; Rivers, 1997, 2008; Rivers et al., 2002). Moreover, U–Pb dating on metamorphic minerals from the Havre-Saint-Pierre complex reveals a metamorphic phase around 1062 Ma and monazites in paragneiss have been dated between 1063 and 1047 Ma (Wodicka et al., 2003). The similarity of the ages for the crystallization of the Havre-Saint-Pierre anorthosite and the Ottawan metamorphic peak is consistent with the very slow cooling rates estimated for the anorthosite (3–4 °C/m.y.r.; Morisset et al., 2009). Based on their Ottawan metamorphic signature, the tectonic unit that includes the Havre-Saint-Pierre anorthosite complex has been included in the allochtonous medium to low pressure belt of the Grenville orogen, characterized by penetrative metamorphism under a relatively high geothermal gradient followed by slow cooling (Rivers, 2008).

During the slow cooling of the Havre-Saint-Pierre anorthosite complex, textural equilibration of the Allard ore took place and ilmenite recrystallized into large polygonal grains. This example of textural coarsening (e.g. Higgins, 1998) is supported by the smaller size of ilmenite grains where included in plagioclase and preserved from recrystallization. Aluminous spinel has also exsolved and migrated to grain boundaries during recrystallization to form external

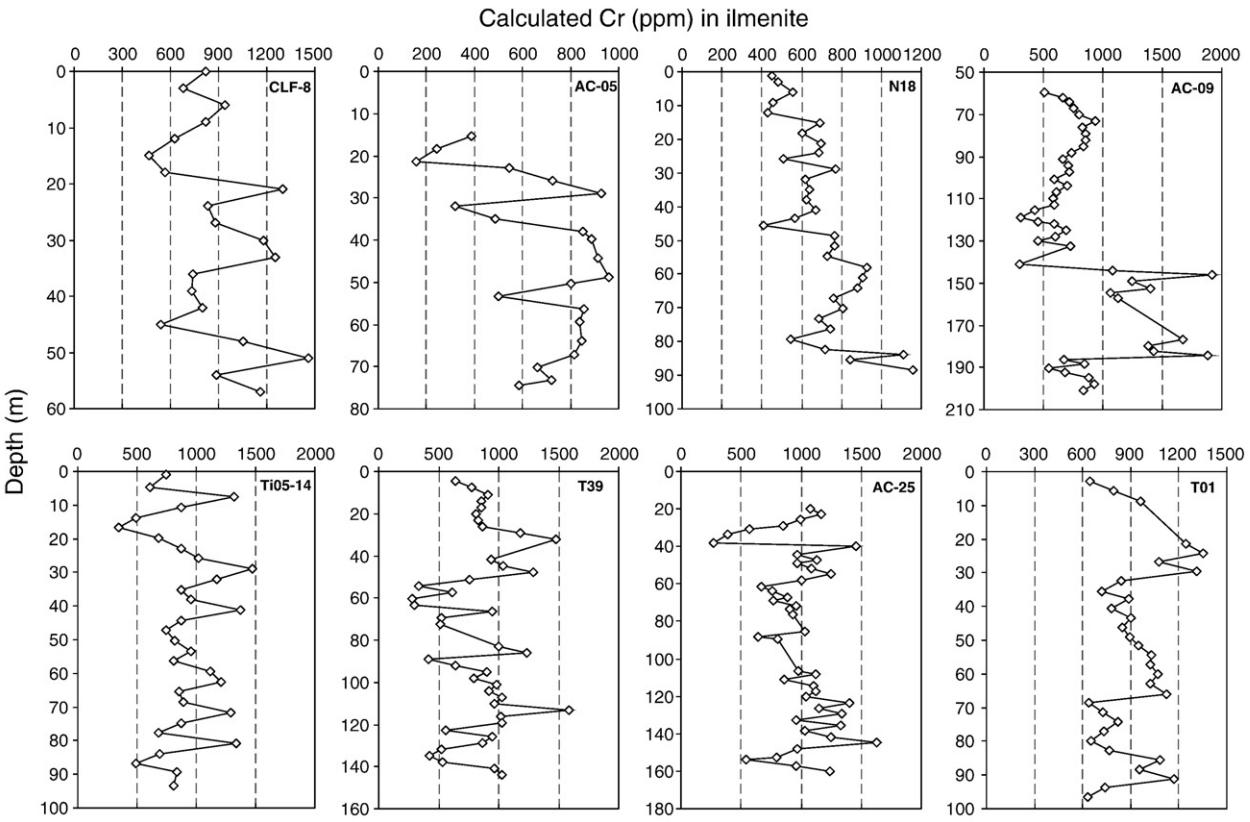

Fig. 13. Calculated Cr concentration in ilmenite (ppm) in selected holes of the Allard Lake ilmenite deposit. The calculation is based on whole-rock TiO_2 and Cr contents and an average TiO_2 content in ilmenite of 37.71 wt.%.

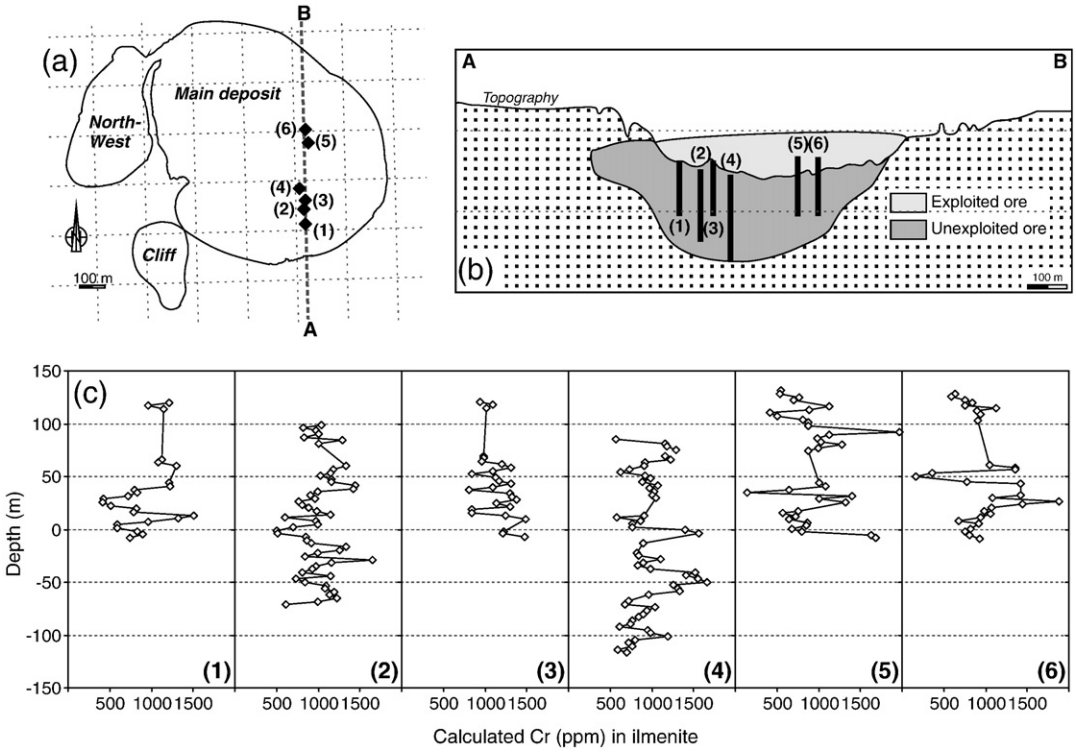

Fig. 14. Stratigraphic variation of the calculated Cr concentration in ilmenite in six selected drill-cores. (a) Surface outline of the open-pit with location of the six selected drill-cores and the South–North A–B cross section; (b) South–North (A–B) cross section in the deposit showing the position of the six drill-cores; (c) Stratigraphic variation of the calculated Cr concentration in ilmenite (ppm) in holes 1 to 6.

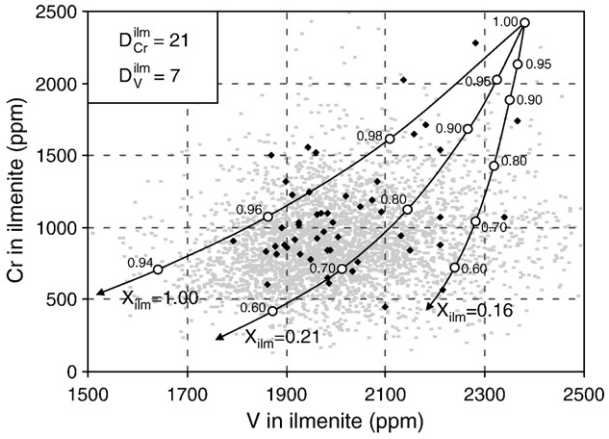

Fig. 15. Cr (ppm) as a function of V (ppm) in ilmenite from the Allard Lake ilmenite deposit with Rayleigh fractional crystallization models for $X_{ilm}=1$ (fractionation of ilmenite alone) and fractionation of a cotectic ilmenite-plagioclase cumulate with $X_{ilm}=0.21$ and 0.16 using a starting composition of ilmenite with Cr = 2415 ppm and V = 2380 ppm. Note the values for the fraction of residual liquid on crystallization paths. Partition coefficients from Charlier et al. (2008). Black symbols represent ilmenite composition from mineral separates and grey points are calculated ilmenite compositions from the whole-rock mining database.

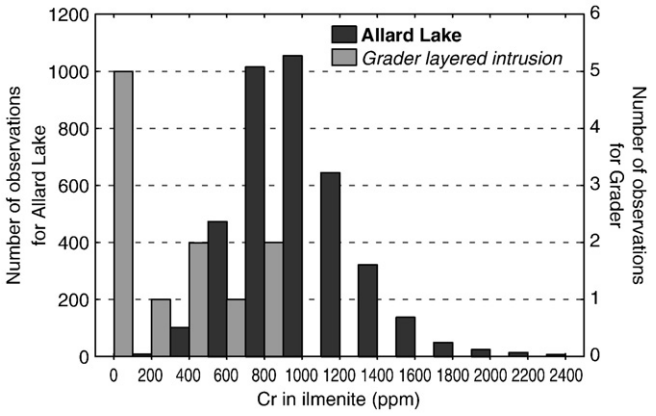

Fig. 16. Histograms of the Cr content in ilmenite (ppm) in the Allard Lake ilmenite deposit compared to that in the Grader layered intrusion (data from Charlier et al., 2008).

granules. The exsolved spinel continued to reequilibrate with adjacent ilmenite grains, as shown by the zoning of aluminous spinel from Fe-rich cores to Mg-rich rims (Fig. 10).

Moreover, in the Allard Lake deposit, two types of orthopyroxene have been described: (1) primary magmatic low-alumina orthopyroxene, common in the anorthosite and some ores, and (2) high-alumina orthopyroxene associated with sapphirine and spinel, detected only in a few samples. Sapphirine has also been described in an ilmenite-rich dyke in the Havre-Saint-Pierre anorthosite close to the Big Island Lake (Bergeron, 1986; Morisset et al., submitted for publication). These rocks also contain large amounts of rutile (up to 15 wt.%), some spinel and corundum. The sapphirine–rutile–ilmenite rocks of the Havre-Saint-Pierre anorthosite are similar to those described in the St-Urbain anorthosite (Warren, 1912; Dymek, 1984; Morisset et al., submitted for publication). High-alumina orthopyroxene and sapphirine are interpreted as resulting from subsolidus reactions of low-alumina orthopyroxene with spinel previously exsolved from ilmenite during slow cooling.

8. Conclusions

The genesis of world-class deposits, including Fe–Ti oxide ores, is a result of exceptional processes that give rise to unusual concentrations of ore–minerals. Although the petrogenesis and emplacement of massif-type anorthosites that host Fe–Ti oxide ore deposits have been investigated for decades, the early saturation of ilmenite in parental liquids to andesine anorthosite (after plagioclase and before ferromagnesian silicates) has only been recognized quite recently. While immiscibility is discarded as an explanation to produce ilmenite ore (Lindsley, 2003), early saturation of ilmenite, accompanied by plagioclase flotation in a dense ferrobasaltic melt, such as in the Tellnes deposit (Charlier et al., 2007), is nevertheless not adequate to explain the formation of the huge amount of massive ilmenite in the Allard Lake deposit. New data on ilmenite and whole-rock compositions from this deposit that are presented here demonstrate intermittent crystallization of ilmenite as the sole liquidus mineral and its accumulation in a magma conduit. The crystallization of ilmenite alone resulted from magma mixing that produced hybrid magmas located in the stability field of ilmenite. These processes explain the geochemical features of the Allard deposit: small scale normal and reverse trends in compatible elements in ilmenite.

Acknowledgements

Rio Tinto Iron and Titanium is thanked for access to their database and to publish the data. Martin Sauvé and Tommy are thanked for their assistance during fieldwork. G Bologne and HJ Bernhardt supervised XRF and microprobe analyses respectively. Comments by Kerry Stanaway and Brian Robins have been greatly appreciated. Andrew Kerr is thanked for the editorial handling. This paper has benefited from the constructive reviews by Brian O'Driscoll and Chusi Li.

References

Andersen, D.J., Lindsley, D.H., Davidson, P.M., 1993. QUILF: a PASCAL program to assess equilibria among Fe–Mg–Ti oxides, pyroxenes, olivine, and quartz. Computers & Geosciences 19, 1333–1350.
Bateman, A.M., 1951. The formation of late magmatic oxide ores. Economic Geology 46, 404–426.
Bergeron, M.B., 1986. Minéralogie et géochimie de la suite anorthositique de la région du Lac Allard, Québec: Evolution des membres mafiques et origine des gîtes massifs d'ilménite, PhD Thesis, University of Montreal, 480 pp.
Bourret, W., 1949. Aeromagnetic survey of the Allard Lake district, Quebec. Economic Geology 44, 732–740.
Campbell, I.H., Murck, B.W., 1993. Petrology of the G and H chromitite zones in the Mountain View area of the Stillwater Complex, Montana. Journal of Petrology 34, 291–316.
Carmichael, C.M., 1959. Remanent magnetism of the Allard Lake ilmenites. Nature 183, 1239–1241.
Charlier, B., Duchesne, J.-C., Vander Auwera, J., 2006. Magma chamber processes in the Tellnes ilmenite deposit (Rogaland Anorthosite Province, SW Norway) and the formation of Fe–Ti ores in massif-type anorthosites. Chemical Geology 234, 264–290.
Charlier, B., Skår, Ø., Korneliussen, A., Duchesne, J.-C., Vander Auwera, J., 2007. Ilmenite composition in the Tellnes Fe–Ti deposit, SW Norway: fractional crystallization, postcumulus evolution and ilmenite–zircon relation. Contributions to Mineralogy and Petrology 154, 119–134.
Charlier, B., Sakoma, E., Sauvé, M., Stanaway, K., Vander Auwera, J., Duchesne, J.-C., 2008. The Grader layered intrusion (Havre-Saint-Pierre Anorthosite, Quebec) and genesis of nelsonite and other Fe–Ti–P ores. Lithos 101, 359–378.
Charlier, B., Namur, O., Duchesne, J.-C., Wiszniewska, J., Parecki, A., Vander Auwera, J., 2009. Cumulate origin and polybaric crystallization of Fe–Ti oxide ores in the Suwalki anorthosite, Northeastern Poland. Economic Geology 104, 205–221.
Charlier, B., Storme, J.-Y., Maquil, R., Vander Auwera, J., Longhi, J., Duchesne, J.-C., submitted for publication. Continuous polybaric fractional crystallization of high-alumina basalt parental magmas in the Egersund–Ogna massif-type anorthosite (Rogaland, SW Norway): constraints from plagioclase and high-alumina orthopyroxene megacrysts.
Corrigan, D., van Breemen, O., 1997. U–Pb age constraints for the lithotectonic evolution of the Grenville Province along the Mauricie transect, Quebec. Canadian Journal of Earth Sciences 34, 299–316.
Corriveau, L., Perreault, S., Davidson, A., 2007. Prospective metallogenic settings of the Grenville Province. In: Goodfellow, W.D. (Ed.), Mineral Deposits of Canada: a Synthesis of Major Deposit-types, District Metallogeny, the Evolution of Geological Provinces, and Exploration Methods: Geological Survey of Canada, Mineral Deposits Division, Special Publication, pp. 819–847.
Davidson, A., 1995. A review of the Grenville orogen in its North American type area. Journal of Australian Geology and Geophysics 16, 3–24.

Davidson, A., 2008. Late Paleoproterozoic to mid-Neoproterozoic history of northern Laurentia: an overview of central Rodinia. Precambrian Research 160, 5–22.
De Waal, S.A., Xu, Z., Li, C., Mouri, H., 2004. Emplacement of viscous mushes in the Jinchuan ultramafic intrusion, western China. Canadian Mineralogist 42, 371–392.
Duchesne, J.C., 1999. Fe–Ti deposits in Rogaland anorthosites (South Norway): geochemical characteristics and problems of interpretation. Mineralium Deposita 34, 182–198.
Duchesne, J.C., Bologne, G., 2009. XRF major and trace element determination in Fe–Ti oxide minerals. Geologica Belgica 12, 205–212.
Dymek, R.F., 1984. Sapphirine of possible igneous origin from the St-Urbain anorthosite massif, Quebec. EOS 65, 295.
Dymek, R.F., 2001. Observations on the Allard Lake anorthosite, Grenville Province, Quebec, and implications for petrogenesis of the CRUML belt of massif anorthosites. Geological Society of America Abstracts with Programs 33, 57.
Dymek, R.F., Owens, B.E., 2001. Petrogenesis of apatite-rich rocks (nelsonites and oxide-apatite gabbronorites) associated with massif anorthosites. Economic Geology 96, 797–815.
Emslie, R.F., 1975. Pyroxene megacrysts from anorthositic rocks: a new clue to the sources and evolution of the parent magmas. Canadian Mineralogist 13, 138–145.
Emslie, R.F., 1985. Proterozoic anorthosite massifs. In: Tobi, A.C., Touret, J.L.R. (Eds.), The Deep Proterozoic Crust in the North Atlantic Provinces. Reidel, Dordrecht, pp. 39–60.
Emslie, R.F., Hunt, P.A., 1990. Ages and petrogenetic significance of igneous mangerite charnockite suites associated with massif anorthosites, Grenville Province. Journal of Geology 98, 213–231.
Force, E.R., 1991. Geology of Titanium-mineral deposits. US Geological Survey Special Paper. 112 pp.
Gobeil, A., Brisebois, D., Clark, T., Verpaelst, P., Madore, L., Wodicka, N., Chevé, S., 2003. Géologie de la moyenne Côte-Nord. In: Brisebois, D., Clark, T. (Eds.), Géologie et ressources minérales de la partie est de la Province de Grenville. Ministère des Ressources naturelles, de la Faune et des Parcs, Québec, pp. 9–58. DV 2002-03.
Hammond, P., 1952. Allard Lake ilmenite deposits. Economic Geology 47, 634–649.
Hargraves, R.B., 1959. Magnetic anisotropy and remanent magnetization in hemo-ilmenite from ore deposits of Allard Lake, Quebec. Journal of Geophysical Research 64, 1565–1573.
Hargraves, R.B., 1962. Petrology of the Allard Lake anorthosite suite, Quebec. In: Engel, A.E.J., James, H.L., Leonard, B.F. (Eds.), Petrologic studies: a volume to honor A.F. Buddington. Geological Society of America, Denver, pp. 163–189.
Hébert, C., Cadieux, A.-M., van Breemen, O., 2005. Temporal evolution and nature of Ti–Fe–P mineralization in the anorthosite–mangerite–charnockite–granite (AMCG) suites of the South–central Grenville Province, Saguenay – Lac St. Jean area, Quebec, Canada. Canadian Journal of Earth Sciences 42, 1865–1880.
Higgins, M.D., 1998. Origin of anorthosite by textural coarsening: quantitative measurements of a natural sequence of textural development. Journal of Petrology 39, 1307–1323.
Higgins, M.D., van Breemen, O., 1996. Three generations of Anorthosite–Mangerite–Charnockite–Granite magmatism, contact metamorphism and tectonism in the Saguenay – Lac–St-Jean region, Grenville Province, Canada. Precambrian Research 79, 347–362.
Hocq, M., 1982. Région du Lac Allard. Ministère de l'Energie et Ressources, Québec. DPV-894, 99 pp.
Icenhower, J.P., Dymek, R.F., Weaver, B.L., 1998. Evidence for an enriched mantle source for jotunite (orthopyroxene monzodiorite) associated with the St. Urbain anorthosite, Quebec. Lithos 42, 191–212.
Irvine, T.N., 1975. Crystallization sequences in the Muskox intrusion and other layered intrusions — II. Origin of chromitite layers and similar deposits of other magmatic ores. Geochimica et Cosmochimica Acta 39, 991–1020.
Irvine, T.N., 1977. Origin of chromitite layers in the Muskox intrusion and other stratiform intrusions: a new interpretation. Geology 5, 273–277.
Kinnaird, J.A., Kruger, F.J., Nex, P.A.M., Cawthorn, R.G., 2002. Chromitite formation — a key to understanding processes of platinum enrichment. Transactions of the Institution of Mining and Metallurgy 111, 23–35.
Klemme, S., Gunther, D., Hametner, K., Prowatke, S., Zack, T., 2006. The partitioning of trace elements between ilmenite, ulvospinel, armalcolite and silicate melts with implications for the early differentiation of the moon. Chemical Geology 234, 251–263.
Kolker, A., 1982. Mineralogy and geochemistry of Fe–Ti oxide and apatite (nelsonite) deposits and evaluation of the liquid immiscibility hypothesis. Economic Geology 77, 1146–1158.
Li, C., Naldrett, A.J., 1999. Geology and petrology of the Voisey's Bay intrusion: reaction of olivine with sulfide and silicate liquids. Lithos 47, 1–31.
Li, C.S., Xu, Z.H., de Waal, S.A., Ripley, E.M., Maier, W.D., 2004. Compositional variations of olivine from the Jinchuan Ni–Cu sulfide deposit, western China: implications for ore genesis. Mineralium Deposita 39, 159–172.
Lindsley, D.H., 2003. Do Fe–Ti oxide magmas exist? Geology: yes; Experiments: no! Norges Geologiske Undersøkelse Special Publication 9, 34–35.
Lister, G.F., 1966. The composition and origin of selected iron–titanium deposits. Economic Geology 61, 275–310.
Longhi, J., Vander Auwera, J., Fram, M., Monthieth, J.N., 1993. Pressure effects, kinetics and rheology of anorthositic and related magmas. American Mineralogist 78, 1016–1030.
Maier, W.D., Li, C., De Waal, S.A., 2001. Why are there no major Ni–Cu sulfide deposits in large layered mafic–ultramafic intrusions? Canadian Mineralogist 39, 547–556.
McEnroe, S.A., Robinson, P., Langenhorst, F., Frandsen, C., Terry, M.P., Boffa Ballaran, T., 2007. Magnetization of exsolution intergrowths of hematite and ilmenite: mineral chemistry, phase relations, and magnetic properties of hemo-ilmenite ores with micron- to nanometer-scale lamellae from Allard Lake, Quebec. Journal of Geophysical Research 112, B10103.
Morisset, C.-E., Scoates, J.S., 2008. Origin of zircon rims around ilmenite in mafic plutonic rocks of Proterozoic anorthosite suites. Canadian Mineralogist 46, 289–304.
Morisset, C.-E., Scoates, J.S., Weis, D., Friedman, R.M., 2009. U–Pb and $^{40}Ar/^{39}Ar$ geochronology of the Saint-Urbain and Lac Allard (Havre-Saint-Pierre) anorthosites and their associated Fe–Ti oxide ores, Québec: evidence for emplacement and slow cooling during the collisional Ottawan orogeny in the Grenville Province. Precambrian Research 174, 95–116.
Morisset, C.-E., Scoates, J.S., Weis, D., Sauvé, M., Stanaway, K., submitted for publication. Rutile-bearing ilmenite deposits associated with Proterozoic massifs of the Grenville Province (Québec). Canadian Mineralogist.
Owens, B.E., Dymek, R.F., 2001. Petrogenesis of the Labrieville alkalic anorthosite massif, Grenville Province, Quebec. Journal of Petrology 42, 1519–1546.
Owen, J.V., Greenough, J.D., 1991. An empirical sapphirine-spinel Mg–Fe exchange thermometer and its application to high grade xenoliths in the Popes Harbour dyke, Nova Scotia, Canada. Lithos 26, 317–332.
Owens, B.E., Dymek, R.F., 2005. Rediscovery of the Mattawa anorthosite massif, Grenville Province, Quebec. Canadian Journal of Earth Sciences 42, 1699–1718.
Owens, B.E., Rockow, M.W., Dymek, R.F., 1993. Jotunites from the Grenville Province, Quebec: petrological characteristics and implications for massif anorthosite petrogenesis. Lithos 30, 57–80.
Owens, B.E., Dymek, R.F., Tucker, R.D., Brannon, J.C., Podosek, F.A., 1994. Age and radiogenic isotopic composition of a late- to posttectonic anorthosite in the Grenville Province — the Labrieville massif, Quebec. Lithos 31, 189–206.
Pang, K.-N., Li, C., Zhou, M.-F., Ripley, E.M., 2008. Abundant Fe–Ti oxide inclusions in olivine from the Panzhihua and Hongge layered intrusions, SW China: evidence for early saturation of Fe–Ti oxides in ferrobasaltic magma. Contributions to Mineralogy and Petrology 156, 307–321.
Pang, K.-N., Li, C., Zhou, M.-F., Ripley, E.M., 2009. Mineral compositional constraints on petrogenesis and oxide ore genesis of the late Permian Panzhihua layered gabbroic intrusion, SW China. Lithos 110, 199–214.
Philpotts, A.R., 1967. Origin of certain iron–titanium oxide and apatite rocks. Economic Geology 62, 303–315.
Rivers, T., 1997. Lithotectonic elements of the Grenville Province: review and tectonic implications. Precambrian Research 86, 117–154.
Rivers, T., 2008. Assembly and preservation of lower, mid, and upper orogenic crust in the Grenville Province — implications for the evolution of large hot long-duration orogens. Precambrian Research 167, 237–259.
Rivers, T., Corrigan, D., 2000. Convergent margin on southeastern Laurentia during the Mesoproterozoic: tectonic implications. Canadian Journal of Earth Sciences 37, 359–383.
Rivers, T., Martignole, J., Gower, C.F., Davidson, A., 1989. New tectonic divisions of the Grenville Province, southeastern Canadian Shield. Tectonics 8, 63–84.
Rivers, T., Ketchum, J., Indares, A., Hynes, A., 2002. The high pressure belt in the Grenville Province: architecture, timing, and exhumation. Canadian Journal of Earth Sciences 39, 867–893.
Roeder, P.L., Reynolds, I.M., 1991. Crystallization of chromite and chromium solubility in basaltic melts. Journal of Petrology 32, 909–934.
Romer, R.L., 1996. Contiguous Laurentia and Baltica before the Grenvillian—Sveconorwegian orogeny? Terra Nova 8, 173–181.
Toplis, M.J., Carroll, M.R., 1995. An experimental study of the influence of oxygen fugacity on Fe–Ti oxide stability, phase relations, and mineral-melt equilibria in ferro-basaltic systems. Journal of Petrology 36, 1137–1170.
U.S.G.S., 2010. Mineral commodity summaries 2010. United States Geological Survey. 193 pp.
van Breemen, O., Higgins, M.D., 1993. U–Pb zircon age of the southwest lobe of the Havre-Saint-Pierre Anorthosite Complex, Grenville Province, Canada. Canadian Journal of Earth Sciences 30, 1453–1457.
Warren, C.H., 1912. The ilmenite rock near St. Urbain: a new occurrence of rutile and sapphirine. American Journal of Science 33, 263–277.
Wilson, J.R., Robins, B., Nielsen, F.M., Duchesne, J.C., Vander Auwera, J., 1996. The Bjerkreim-Sokndal layered intrusion, Southwest Norway. In: Cawthorn, R.G. (Ed.), Layered Intrusions. Elsevier, Amsterdam, pp. 231–255.
Wodicka, N., David, J., Parent, M., Gobeil, A., Verpaelst, P., 2003. Géochronologie U–Pb et Pb–Pb de la région de Sept-Îles — Natashquan, Province de Grenville, Moyenne–Côte–Nord. In: Brisebois, D., Clark, T. (Eds.), Géologie et ressources minérales de la partie est de la Province de Grenville. Ministère des Ressources naturelles, de la Faune et des Parcs, Québec, pp. 59–117. DV 2002-03.
Zhou, M.-F., Robinson, P.T., Lesher, C.M., Keays, R.R., Zhang, C.-J., Malpas, J., 2005. Geochemistry, petrogenesis and metallogenesis of the Panzhihua gabbroic layered intrusion and associated Fe–Ti–V oxide deposits, Sichuan Province, SW China. Journal of Petrology 46, 2253–2280.